Chem Soc Rev

Dynamic Article Links

Cite this: *Chem. Soc. Rev.*, 2011, **40**, 3249–3265

www.rsc.org/csr

CRITICAL REVIEW

Microporous magnets†

Pierre Dechambenoit and Jeffrey R. Long*

Received 3rd November 2010
DOI: 10.1039/c0cs00167h

Combining porosity and magnetic ordering in a single material presents a significant challenge since magnetic exchange generally requires short bridges between the spin carriers, whereas porosity usually relies on the use of long diamagnetic connecting ligands. Despite this apparent incompatibility, notable successes have been achieved of late in generating truly microporous solids with high magnetic ordering temperatures. In this *critical review*, we give an overview of this emerging class of multifunctional materials, with particular emphasis on synthetic strategies and possible routes to new materials with improved properties (149 references).

1. Introduction

The development of new advanced materials more and more requires the combination of different properties within the same material. Most interesting are properties that can interact mutually to result in cooperative effects. Among such multifunctional materials, the combination of magnetism and porosity attracted considerable interest this past decade.[1–4] Possible uses of these materials include as magnetic sensors, low-density magnets, or magnetic separation media. Indeed, the magnetic flux within the pores of the solid is expected to attract selectively paramagnetic molecules while repelling diamagnetic molecules, potentially enabling the separation of dioxygen from air through a noncryogenic process. Additional functionalities can also be supplied by functional molecules encapsulated within the pores of the magnetic solid.

Department of Chemistry, University of California, Berkeley, CA 94720-1460, USA. E-mail: jrlong@berkeley.edu; Fax: +1 510 643 3546; Tel: +1 510 642 0860

† Part of the molecule-based magnets themed issue.

Several reviews dealing with open magnetic frameworks have already been published.[1–4] Here, we will mainly focus on compounds that exhibit both long-range magnetic order and well-established porosity, as demonstrated through the reversible uptake of host molecules (either as a gas or a liquid). Employing relevant examples, we will particularly emphasize the strategies that can be used for the formation of microporous magnets and for their future improvements.

Extraordinary advances in porous materials have been made over the last two decades through the incorporation of molecular components as tunable connectors between metal nodes. A large number of porous hybrid organic/inorganic compounds or metal–organic frameworks have thus been obtained with very high porosity and the capability of hosting a myriad of guests, including gases for storage or separation purposes.[5–9] Simply using paramagnetic metal centers or organic radical bridging ligands in the assembly of such solids provides the first step towards creation of a microporous magnet. However, the formation of a permanent magnet additionally requires that these spin carriers be in intimate contact. The critical ordering temperature (T_c) for the material

Pierre Dechambenoit

Pierre Dechambenoit was born in Mulhouse, France, in 1982. He received a PhD in 2008 under the supervision of Prof. Mir Wais Hosseini and Dr Sylvie Ferlay in Strasbourg, working in the field of supramolecular chemistry. Following postdoctoral work on magnetic coordination clusters and porous conductors at UC Berkeley, he has recently taken up a position on the faculty at the University of Bordeaux.

Jeffrey R. Long

Jeffrey R. Long was born in Rolla, Missouri (USA), in 1969. He received a BA from Cornell University in 1991 and a PhD from Harvard University in 1995. Following postdoctoral work at Harvard and the University of California, Berkeley, he joined the faculty at Berkeley in 1997. His research involves the synthesis of new inorganic clusters and solids with emphasis on magnetic and microporous materials.

correlates with the strength of these magnetic interactions, together with the number of nearest paramagnetic neighbours.[10] Importantly, the strength of the magnetic coupling is highly dependent on the number and type of bridging atoms between the spin carriers. Indeed, while one-atom oxido bridges can result in ordering temperatures of up to 900 K, compounds with two-, three- or four-atom bridges do not exceed 350, 50, and 2 K respectively.[1] Therefore, with the exception of some intriguing and promising cases which will be discussed later,[11–14] organic spacers usually do not mediate a strong magnetic coupling between the metal centers. Nevertheless, the various possible coordination modes of the organic linkers and the potential for tailoring them can provide a rich chemistry and possible means of controlling and tuning both the porosity and the magnetic properties. Several additional properties can also come from these organic molecules or their interaction with the metal centers, including thermochromism, photochromism, and photomagnetism.

Among the possible ways to classify porous materials, Férey introduced a classification according to the dimensionality of the inorganic (sub)network,[15] ranging from 3-D for purely inorganic materials, to 0-D for coordination polymers or purely organic materials, *via* 2-D and 1-D for hybrid organic–inorganic materials, such as pillared inorganic layers or inorganic chains linked by organic bridges. This classification is well adapted for the case of porous magnet since the magnetism can often be discussed as a function of the dimensionality of the inorganic subnetwork. Indeed, whereas most of the common inorganic bridges involve few atoms—such as oxide, hydroxide, or cyanide—organic bridges usually involve several atoms, such that the magnetic coupling is much weaker or even negligible. In addition to the inorganic dimensionality, the overall dimensionality (and therefore the organic one) is of highest importance for the porosity. Rao and Cheetham *et al*. introduced a simple notation to describe both the inorganic and organic dimensionality of a structure, as the form I^mO^n where m and n represent the dimensionality of the inorganic and organic connectivity, respectively.[4,16] For instance, purely 3-D inorganic structures are denoted I^3O^0 whereas inorganic layers pillared by organic linkers are denoted I^2O^1. A description of representative examples of microporous magnetic materials belonging to each of these four classes is given next. We then close with a discussion of some possible strategies for creating new examples of microporous magnets with enhanced properties.

2. Porous magnets based on 3-D inorganic subnetworks (I^3O^n)

By far the majority of microporous magnetic solids with a 3-D inorganic subnetwork are based on oxygen or cyanide bridges between paramagnetic metal centers.

Typical oxygen-bridged solids include oxides, hydroxides, phosphates, phosphites, sulfates, and carboxylates. Most are therefore purely inorganic and their syntheses and properties are similar to those of zeolites. Generally, the formation of such compounds is carried out under hydro- or solventothermal conditions by using organic amines/ammonium or alkali metal cations as templates or structure-directing agents. A very large number of magnetic inorganic open frameworks have been obtained by such means. However, the organic templates often cocrystallize within the pores of the solid, and display strong interactions with the inorganic framework. As a consequence, their removal is challenging and frequently results in collapse of the framework.

Despite this, several porous magnetic inorganic frameworks have been reported. Among the most beautiful examples are the nickel(II) phosphates $Ni_{18}[(HPO_4)_{14}(OH)_3F_9(H_3O/NH_4)_4]\cdot 12H_2O$ and $Ni_{20}[(OH)_{12}(H_2O)_6][(HPO_4)_8(PO_4)_4]\cdot 12H_2O$, respectively, known as VSB-1[17] and VSB-5.[18] These compounds were synthesized hydrothermally starting from nickel chloride, phosphoric acid, and fluoride sources for VSB-1 such as HF, NH_4F, or KF. Several types of amines were also originally used, but the synthesis can also be performed without amines under microwave irradiation.[19,20] The structures of both compounds are based upon the interconnection of octahedral NiO_6 through oxygen bridges, forming a 3-D Ni–O–Ni network presenting large 24-membered ring channels with respective diameters of 8.8 and 10.2 Å for VSB-1 and VSB-5 (Fig. 1).

Here, the 1-D channels are filled with water molecules, but these can be removed upon calcination in air at 350 °C, affording microporous solids with a BET surface area of 180 $m^2\ g^{-1}$ for VSB-1 and up to 500 $m^2\ g^{-1}$ for VSB-5. The large pores that result have been successfully used for catalysis,[18,21–23] ion exchange,[17,24] and hydrogen storage.[25]

Magnetic susceptibility and magnetization measurements revealed a canted antiferromagnetic ordering below 10.5 K for VSB-1 with a Curie–Weiss constant θ of −71 K. The compound VSB-5 orders antiferromagnetically below 14 K with $\theta = -49.5$ K. A second magnetic transition at about 6 K is also observed, which possibly involves spin canting. Interestingly, both the nickel centers and the phosphorus atoms belonging to the phosphates can be partially substituted by other metallic cations, such as Fe, Co, Mn, Zn, or V.[17,26–29] As a consequence of this doping, the magnetic properties are affected. In particular, the ordering temperature can be increased from 10.5 K to 20 K by doping VSB-1 with 10% Fe.[17]

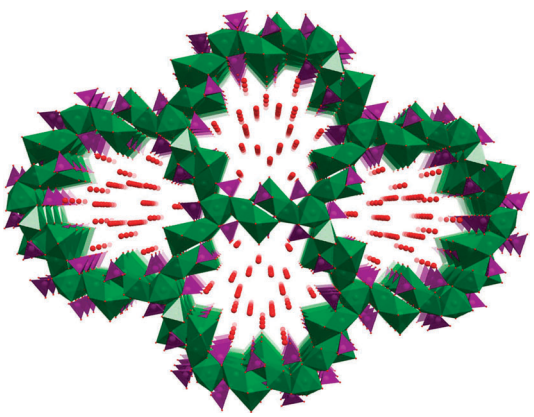

Fig. 1 Polyhedral representation of a portion of the crystal structure of VSB-5 showing the 1-D channels filled by water molecules. Green and purple spheres in the center of green octahedral and purple tetrahedral represent Co and P atoms, respectively; polyhedra corners and red spheres represent O atoms; H atoms are omitted for clarity.

Other magnetic porous phosphates have been reported, such as $[Fe_4F_3(PO_4)_4](C_6H_{14}N_2)$ (ULM-19),[30,31] and $[Fe_2(OH)(H_2O)(PO_4)_2](NH_4)(H_2O)$.[32] The structure of ULM-19 is based upon the interconnection of mononuclear iron centers and fluoride-bridged trinuclear iron clusters through phosphate groups (Fe–O–P–O–Fe), whereas $[Fe_2(OH)(H_2O)(PO_4)_2](NH_4)(H_2O)$ is composed of oxygen-bridged tetranuclear iron clusters connected through phosphate groups (Fe–O–P–O–Fe). Both compounds behave as antiferromagnets with T_N = 9 and 22 K, respectively.

Like tetrahedral phosphate groups, pseudopyramidal hydrogen phosphite units HPO_3^{2-} can also be used for the formation of porous frameworks. Recently, a nickel phosphite exhibiting large pores was reported in the form of $[Ni_8(HPO_3)_9Cl_3](H_3O)_5(H_2O)_{1.5}$.[33] Interestingly, the synthesis of this compound from nickel chloride and phosphorous acid was performed ionothermally in the ionic liquid (Pmim)(PF_6). The crystal structure consists of an anionic framework of formula $[Ni_8(HPO_3)_9Cl_3]^{5-}$, which forms large 18-membered ring 1-D channels with a diameter of *ca.* 11 Å (Fig. 2a). These channels are filled with protonated water molecules for charge balance, as well as by free water molecules that can be removed upon heating. The 3-D open anionic framework is built up by the interconnection of edge- and face-sharing NiO_6 and NiO_5Cl octahedra through oxygen bridges, forming 2-D Ni–oxygen/chloride networks, which are stacked and pillared by HPO_3^{2-} pseudopyramidal groups (Fig. 2b). Magnetic measurements revealed that the paramagnetic nickel(II) centers are coupled ferromagnetically within the Ni–oxygen/chloride layers through the oxygen bridges. A spin flop transition at 20 kOe is observed only when the applied field is perpendicular to the layers, indicating that the easy axis is oriented along this direction. In other words, the magnetic moments within a single layer orient along the same direction (the *c* axis) at zero field due to the magnetic anisotropy. Below 8.5 K, these ferromagnetic layers stack antiferromagnetically along the *c* axis through a weak Ni–O–P–O–Ni superexchange pathway, giving an overall 3-D antiferromagnet. Even if this compound is purely inorganic (I^3O^0), it is similar topologically and magnetically to the organically pillared inorganic layers (I^2O^1) discussed below.

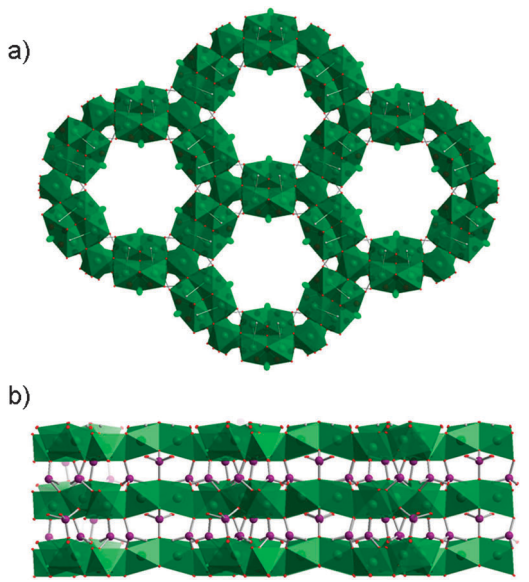

Fig. 2 Polyhedral representation of a portion of the crystal structure of the anionic framework $[Ni_8(HPO_3)_9Cl_3]^{5-}$ in $[Ni_8(HPO_3)_9Cl_3](H_3O)_5(H_2O)_{1.5}$ (a) along the (*ab*) plane showing the 1-D channels, (b) showing the stacking of the inorganic layers along the *c* axis. Dark green spheres in the center of green octahedral represent Co atoms; light green and purple spheres represent Cl and P atoms respectively; the red corners of the octahedra represent O atoms; H atoms are omitted for clarity.

Besides these purely inorganic compounds, carboxylates can also form 3-D inorganic M–O–M subnetworks. Of particular interest for this topic is the family of isostructural porous formates $M_3(HCOO)_6$, where M = Fe, Co, Mn, Ni.[34–44] The structure is based on edge- and corner-sharing of octahedral metal centers forming a 3-D diamondoid framework with 1-D channels (diameter *ca.* 4 × 5 Å). The framework can also be seen as built up from MM_4 tetrahedral nodes formed *via* connection of a central metal ion to four other metal ions by both one- and three-atoms formate bridges (M–O–M and M–O–C–O–M), each formate connecting three metal centers through a *syn–syn*/*anti* coordination mode (Fig. 3a and b).

The solvent molecules filling the 1-D channels can be removed under reduced pressure or by heating without damage to the framework. Very remarkably, the resulting pores can be refilled by a myriad of guests, such as gases (H_2, CO_2, *etc.*), liquids (both polar and apolar: DMF,

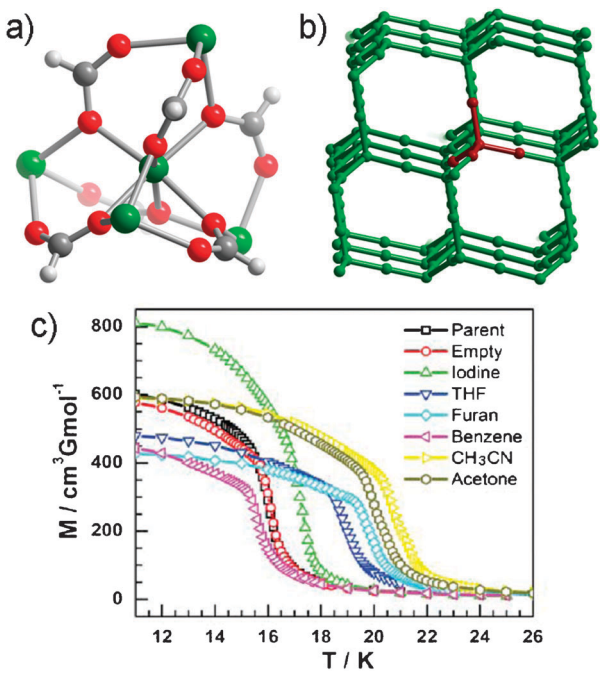

Fig. 3 (a) Portion of the crystal structure of $M_3(HCOO)_6$ showing the MM_4 tetrahedron node. Green, gray, red, and white spheres represent M, C, O, and H atoms respectively. (b) Representation of the porous diamondoid framework with one MM_4 tetrahedron highlighted in red. (c) Field-cooled magnetization data for $[Fe_3(HCOO)_6]$ (“Empty”) and its guest-inclusion compounds under an applied field of 10 Oe. The as-synthesized form of the compound with methanol and water guest molecules is designated “Parent”. Adapted from ref. 44, copyright The Royal Society of Chemistry 2008.

acetonitrile, benzene, *etc.*) and solids (imidazole). Such a diversity of guests is possible owing to the flexibility of the framework, with variation of the lattice volume of up to 11% upon guest inclusion,[41] and the amphiphilic character of the channels (the inner walls are lined by alternate arrays of C–H groups and oxygen atoms).

Despite possessing a three-dimensional M–O–M network, the magnetic ordering temperatures of these compounds are quite low, and dependent on the nature of the metal centers: the Fe, Mn and Ni compounds are ferrimagnets with T_c = 16.1, 8.0, and 2.7 K, respectively, whereas the Co compound is probably a spin-canted antiferromagnet below 1.8 K. The Mn and Ni compounds are further soft magnets while the Fe compound is quite hard. Guest-dependent magnetism has been investigated systematically for the Mn and Fe frameworks (Fig. 3c). Significant guest-modulated ordering temperatures have been observed, ranging from 15.6 to 20.7 K with Fe and 4.8 to 9.7 K with Mn.[35] For Fe, a higher T_c has also been shown to be commensurate with an increase of both the coercive field (H_c) and a remnant magnetization (M_r), reaching up to H_c = 3400 Oe and M_r = 5.4 μ_B at 1.8 K for $Fe_3(HCOO)_6{\cdot}CH_3CN$, compared to H_c = 700 Oe and M_r = 4.0 μ_B without guest.[39]

Magnetic properties can also be affected by doping with diamagnetic metal ions. A series of solid solutions of the formula $Fe_xZn_{3-x}(HCOO)_6$ have been synthesized with x = 0.26, 1.03, 1.78, 2.22, and 2.43. Upon increasing the diamagnetic component Zn, the series exhibits systematic changes from long-range three-dimensional ordering to spin glass to superparamagnet or possible single-molecule magnet (a large frequency dependence has been observed in ac magnetic susceptibility measurements) and finally to paramagnet.[40] Solvent dependent ferroelectricity has also been reported with Mn, forming therefore a remarkable example of a molecule-based multiferroic material.[42,43]

Several other intriguing open magnetic metal formates with different topologies have been reported. These can include amines[41] or CO_2[45,46] acting as templates for their synthesis. However, even for the latter, the CO_2 molecules trapped within the pores of a 3-D cubic M–O–C–O–M (M = Mn or Fe) bridged network cannot be removed without collapsing the framework, perhaps due to strong interactions with the framework through multiple C–H···O hydrogen bonds.

Another porous carboxylate-based 3-D inorganic network is the nickel glutarate $Ni_{20}(C_5H_6O_4)_{20}(H_2O)_8$ (MIL-77).[47] The as-synthesized product, of formula $Ni_{20}(C_5H_6O_4)_{20}(H_2O)_8{\cdot}40H_2O$, is built up from a 3-D network of edge sharing Ni octahedra with water ligands and features corrugated crossing 20-membered ring channels. These channels are filled with the organic skeleton of the glutarate and guest water molecules. The latter can be removed by heating, affording a microporous solid with a BET surface area of 346 $m^2\ g^{-1}$ and which behaves as a ferromagnet below 4 K. Upon dehydration, the structure undergoes a compression of *ca.* 13% of the volume. Such a flexibility is very unusual for a 3-D oxide framework, and is ascribed to the repositioning of some carboxylate groups during the transition and to a very surprising reversible hopping of nickel atoms into the voids of the inorganic skeleton.[48]

One of the major limitations for all such oxo-bridged materials is the difficulty of rationally designing a structure. As for zeolites, the large majority are obtained with an empirical trial-and-error synthesis. This lack of control is in particular due to the large angular flexibility of oxygen bridges (M–O–M). Importantly, the nature of the magnetic exchange coupling (ferro- or antiferromagnetic, as well as the magnitude) also depends upon this bridging angle, as rationalized by the Goodenough–Kanamori rules.[49] As a consequence, both the structure type and the magnetism are difficult to predict. This problem can be circumvented by using a more directional bridging ligand, such as cyanide. Indeed, cyanide is a ligand of choice due to its simplicity, its high directionality and its ability to mediate reasonably strong magnetic coupling. It is therefore widely used for the formation of magnetic materials, from discrete coordination clusters such as single-molecule magnets[50,51] to 3-D magnetic frameworks.

Prussian blue analogues

Prussian blue analogues are the most known and studied cyanide-based frameworks, and constitute one of the most promising classes of potentially porous magnetic materials. In these compounds, octahedral $[M'(CN)_6]^{x-}$ complexes are linked *via* octahedrally-coordinated, nitrogen-bound M^{y+} ions to give a cubic $M_x[M'(CN)_6]_y$ framework (Fig. 4a and b). Depending on the stoichiometry M′/M and the respective oxidation states, the structure can also contain monocationic counterions, located in the cavities of the cubic structure (Fig. 4b), or $[M'(CN)_6]^{x-}$ vacancies when $x > y$ (Fig. 4a). When such vacancies are present, the available coordination

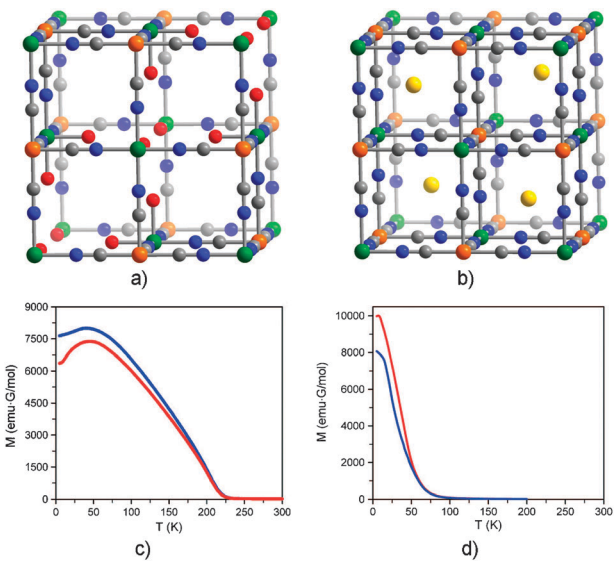

Fig. 4 (a) Portion of the crystal structure of the Prussian blue analogues $M^{II}_3[M'^{III}(CN)_6]_2{\cdot}6H_2O$ and (b) $A^IM^{II}[M'^{III}(CN)_6]$. Yellow, orange, green, gray, blue and red spheres represent A, M, M′, C, N, and O atoms, respectively; H atoms are omitted for clarity. Field-cooled magnetization data collected at 1000 Oe for (c) $Cr_3[Cr(CN)_6]_2{\cdot}6H_2O$ (blue) and (d) $CsNi[Cr(CN)_6]$ (blue), and for samples of the same compounds sealed in quartz tubes containing 2.9 and 1.8 molecules of O_2 per formula unit, respectively (red). Adapted from ref. 70 copyright 2008 American Chemical Society.

sites on M are occupied by bound water molecules (Fig. 4a). Other water or small solvent molecules can also be situated within the pores of the cubic framework. With a suitable choice of the transition metal ions M and M′, a number of Prussian blue analogues with high magnetic ordering temperatures have been elaborated, reaching up to 376 K for $KV[Cr(CN)_6]_2{\cdot}2H_2O$.[52] Furthermore, based on empirical and theoretical studies, the nature (ferro- *versus* antiferro-) and an estimation of the strength of the magnetic coupling through the cyanide bridges can be predicted, facilitating rational design of the magnetic properties of these compounds.[53–55]

Upon dehydration, a large number of Prussian blue analogues exhibiting permanent porosity have also been obtained, with BET surface areas of up to 870 $m^2\ g^{-1}$.[56] These materials have recently been studied for H_2 storage and CO_2 capture due to the wide range of metal centers that can be exposed on their internal surfaces.[8,56–61] Prussian blue itself, $Fe_4[Fe(CN)_6]_3{\cdot}14H_2O$, can be fully dehydrated without collapsing the framework, affording a microporous solid with a surface area of 550 $m^2\ g^{-1}$, which is capable of adsorbing small molecules such as MeOH, N_2, and H_2.[62] The hydrated phase behaves as a ferromagnet with a Curie temperature of 5.6 K.[63–65]

However, examples where both microporosity and bulk magnetic ordering have been demonstrated to coexist are still scarce. One of the first example was made from the dehydration of the pentacyanometallate-based ferrimagnet $Co_3[Co(CN)_5]_2{\cdot}8H_2O$.[66] Remarkably, the resulting microporous magnet shows a hysteresis loop at 5 K with H_c = 1160 Oe and M_r = 745 cm^3 Oe mol^{-1} (compared to H_c = 1160 Oe and M_r = 1540 cm^3 Oe mol^{-1} for the hydrated sample). Upon dehydration, the Néel temperature decreases from 48 K to 38 K. The high BET surface area of 730 $m^2\ g^{-1}$ further allows the adsorption of large amounts of gases such as N_2, O_2, and H_2 at 77 K.[56,66]

Conversely, an increase of the ordering temperature upon dehydration has been observed for the ferromagnets $Ni_3[Fe(CN)_6]_2$ (T_c = 24.9 K *vs.* 18.9 K with nH_2O),[67] $Cu_3[Fe(CN)_6]_2$ (T_c = 21.8 K *vs.* 17.9 K with $10H_2O$)[67] and for the ferrimagnets $Mn_3[Fe(CN)_6]_2$ (T_N = 9.9 K *vs.* 7.9 K with nH_2O)[67] and $K_{0.2}Mn_{1.4}[Cr(CN)_6]$ (T_N = 99 K *vs.* 66 K with $6H_2O$).[68] For this last compound, the Néel temperature can be tuned by a partial dehydration.

Dehydration of Prussian blue analogues can also sometimes lead to drastic modifications of the magnetic properties. Partial dehydration of the pink ferromagnet $Co[Cr(CN)_6]_{2/3}(H_2O)_{5.1}$ (T_c = 28 K) gives rise to a blue ferrimagnet of formula $Co[Cr(CN)_6]_{2/3}(H_2O)_{4.2}$ (T_N = 22 K).[69] This spin inversion and solvatochromism are due to the desorption of water molecules coordinated to the Co^{II} centers, changing the coordination geometry from a six-coordinate octahedral Co^{II} center to a four-coordinate tetrahedral Co^{II} center, switching the magnetic coupling with Cr^{III} from ferromagnetic to antiferromagnetic.

The best performing microporous magnets to date are probably $CsNi[Cr(CN)_6]$ and $Cr_3[Cr(CN)_6]_2{\cdot}6H_2O$, which order magnetically at T_c = 75 K and T_N = 219 K respectively.[70] These ordering temperatures are by far the highest reported yet for microporous ferro- and ferrimagnets. These solids were obtained upon dehydration of $CsNi[Cr(CN)_6]{\cdot}2H_2O$ (T_c = 90 K)[71] and $Cr_3[Cr(CN)_6]_2{\cdot}10H_2O$ (T_N = 240 K), and exhibit permanent porosity with BET surface areas of 360 and 400 $m^2\ g^{-1}$, respectively. The six remaining water molecules in $Cr_3[Cr(CN)_6]_2{\cdot}6H_2O$ are most likely coordinated to the Cr^{II} centers (Fig. 4a), but cannot be removed without collapsing the framework, affording an amorphous product without long-range magnetic ordering down to 5 K. These compounds further show remarkable changes in their magnetic properties upon adsorption of O_2. In $Cr_3[Cr(CN)_6]_2{\cdot}6H_2O$, adsorption of O_2 results in a reversible decrease in the magnetic moment of the system (Fig. 4c), as well as a reduction of H_c from 110 to 10 Oe and M_r from 1200 to 400 emu Oe mol^{-1} in the magnetic hysteresis loops collected at 5 K. This indicates a net antiferromagnetic interaction between O_2 and the framework. In $CsNi[Cr(CN)_6]$, adsorption of O_2 instead results in a reversible increase in the magnetic moment of the system, revealing a net ferromagnetic interaction between O_2 and the framework (Fig. 4d).

Other cyano-bridged frameworks

Besides Prussian blue analogues, several other 3-D magnetic cyanide-bridged frameworks have been obtained, some exhibiting porosity.[72–77] An example is the ferrimagnet $[Mn(HL)(H_2O)]_2Mn[Mo(CN)_7]_2{\cdot}2H_2O$ (T_N = 85 K), obtained through the reaction of $[Mo(CN)_7]^{4-}$ with Mn^{2+} ions in the presence of protonated *N*,*N*-dimethylalaninol (L). The latter can be either a racemic mixture, or as a chiral *R*- or *S*-enantiomer, forming therefore chiral magnets.[73] The structure is based on a cyano-bridged 3-D network with 1-D channels that are filled by water molecules (Fig. 5).

Upon heating, both solvate and coordinated water molecules can be reversibly evacuated, affording a microporous solid able to readsorb a modest amount of gases such as N_2, CO_2, and CO. Upon dehydration, the ordering temperature is increased to 106 K (Fig. 5b). This increase in T_N is ascribed to the desorption of one ligating water molecule from a six-coordinate Mn^{II} center, reducing its coordination number and leading to shorter Mn–NC bonds and therefore to stronger Mn···Mo exchange interactions.

Another class of porous magnet is illustrated by the topotactic single crystal-to-single crystal transformation of the 2-D cyano-bridged coordination solid $[Mn(NNdmenH)(H_2O)][Cr(CN)_6]{\cdot}H_2O$ (NNdmen = *N*,*N*-dimethylethylenediamine) to the 3-D framework $[Mn(NNdmenH)][Cr(CN)_6]$ upon dehydration (Fig. 6).[74,75]

The hydrated form of the compound is built up from the connection of four cyanide groups in the equatorial position of $[Cr(CN)_6]^{3-}$ to adjacent Mn^{II} centers, forming a 2-D corrugated sheet structure in the *ab* plane. A protonated ligand and a water molecule are bound at the axial positions of the octahedral Mn^{II} center. The latter is hydrogen bonded to another lattice water molecule as well as to a coordination-free cyano nitrogen atom belonging to the next sheet. As a consequence of the removal of the coordinated water molecule upon heating, additional Mn–NC–Cr bonds are created between the newly available coordination site of the Mn^{II} center and axial cyanides belonging to adjacent sheets, thereby

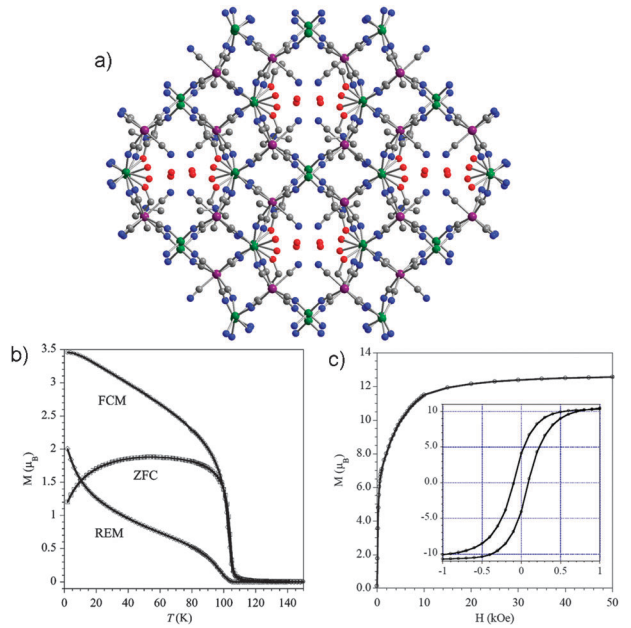

Fig. 5 (a) Portion of the crystal structure of $[Mn(HL)(H_2O)]_2$-$Mn[Mo(CN)_7]_2{\cdot}2H_2O$ (L = (*S*)-*N*,*N*-dimethylalaninol) along the [110] plane, forming 1-D channels along the *c* axis filled by water molecules. Green, purple, gray, blue, and red spheres represent Mn, Mo, C, N, and O atoms, respectively; H atoms are omitted for clarity. (b) Field-cooled magnetization (FCM) data collected at 100 Oe, zero-field cooled (ZFC) magnetization data, and remnant magnetization (REM) as a function of temperature for the fully dehydrated compound $[Mn(HL)]_2Mn[Mo(CN)_7]_2$, showing the onset of the magnetic ordering. (c) Plots of *M vs. H* at 2 K for the dehydrated compound. Inset: hysteresis from −1 to +1 kOe. Adapted from ref. 73 copyright 2007 American Chemical Society.

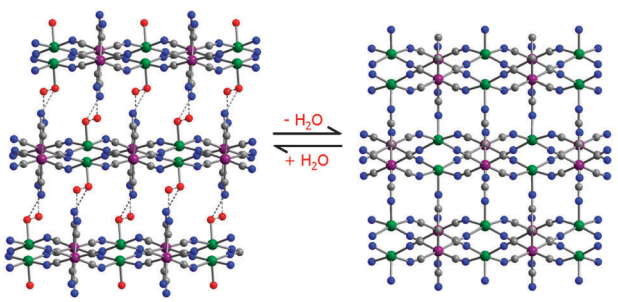

Fig. 6 Portions of the crystal structures of $[Mn(NNdmenH)(H_2O)]$-$[Cr(CN)_6]{\cdot}H_2O$ (left) and $[Mn(NNdmenH)][Cr(CN)_6]$ (right), showing the increase of the dimensionality through the formation of additional cyanide bridges. Purple, green, gray, blue, and red spheres represent Cr, Mn, C, N, and O atoms, respectively; H atoms and NNdmenH molecules are omitted for clarity. Hydrogen bonds are represented by dashed lines.

pillaring the sheets to form a 3-D cyano-bridged network. As a consequence of the increase of the dimensionality, the ordering temperature of these ferrimagnets increases from 35.2 to 60.4 K, and the coercive field increases from 12 to 60 Oe at 2 K. Similar behavior has also been reported recently for the analogues $[Mn(enH)(H_2O)Cr(CN)_6]{\cdot}H_2O$,[76] and $[Mn(pnH)(H_2O)Cr(CN)_6]{\cdot}H_2O$,[77] where en is 1,2-diaminoethane and pn is 1,2-diaminopropane (as a racemate or enantiopure). Notably, this transformation is reversible, as demonstrated by the combined results of variable-temperature X-ray powder diffraction, thermogravimetric analysis, and magnetic measurements. Furthermore, this solid features a high size-selectivity towards the adsorption of solvent vapours. Indeed, adsorption isotherms show a high affinity for H_2O and MeOH, but a negligible uptake of EtOH and MeCN. Contrary to previous examples described in this review, this kind of material does not feature any void space in the dehydrated phase due to the reversible structural transformations. This class of material can be referred as a magnetic sponge[78] or soft porous crystal.[79]

As previously mentioned, the introduction of organic connectors can be an efficient and rational way to introduce porosity. Furthermore, all the possible functionalizations of the organic units can provide numerous additional ways to potentially tune and ultimately control the magnetism and porosity.

3. Porous magnets based on 2-D inorganic subnetworks (I^2O^n)

Few porous magnets featuring 2-D inorganic subnetworks have been reported to date.[80–84] Relevant examples are $Co_4(SO_4)(OH)_6(dabco)_{0.5}{\cdot}H_2O$ (dabco = 1,4-diazabicyclo-[2,2,2]octane) and $Co_4(SO_4)(OH)_6(en)_{0.5}{\cdot}3H_2O$. These compounds possess structures built up from the stacking of inorganic layers formed by edge sharing $Co(OH)_6$ octahedra, regularly decorated by tetrahedral Co^{II} sites located above and below the layers.[81,82] Neutrality is provided by tetrahedral sulfate groups, which share one oxygen atom with the layers. Adjacent layers are linked by pillaring diamines *via* the decorating tetrahedral Co^{II} sites, forming a 3-D network of the type I^2O^1. The void spaces between the layers are filled by hydrogen bonded water molecules which can be reversibly evacuated upon heating to 80 °C. Magnetic measurements performed on the hydrated samples revealed a weak antiferromagnetic exchange between the ferrimagnetic layers with T_N = 14 K for en and 21 K for dabco, together with a small canting. The weak antiferromagnetic coupling between the layers can be overcome by application of a magnetic field (*ca.* 500 Oe for en and 1800 Oe for dabco at 4 K), giving rise to a ferrimagnetic state (metamagnetism). The higher ordering temperature and critical field with dabco can be ascribed to the higher number of magnetic exchange pathways through dabco compared to en (three *vs.* one).

A structurally similar compound is $Co_5(OH)_8(chdc){\cdot}4H_2O$, where $chdc^{2-}$ is *trans*-1,4-cyclohexanedicarboxylate.[83] As for the previous compounds, the structure is built up from inorganic Co^{II}-hydroxide layers decorated by tetrahedral CoO_4 units, which here are linked together by $chdc^{2-}$ pillars through a bis(monodentate) coordination mode (Fig. 7). Upon the reversible evacuation of the water molecules occupying the 1-D channels between the $chdc^{2-}$ pillars, the interlayer spacing undergoes a compression of 9% due to a tilting of the pillars, such that the dehydrated form has no void volume (Fig. 7). The tetrahedral Co^{II} centers are strongly antiferromagnetically coupled with the octahedral ones, forming ferrimagnetic layers. In marked contrast to the

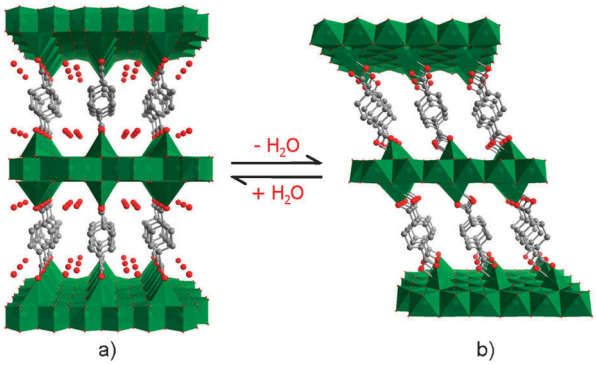

Fig. 7 Polyhedral representation of a portion of the crystal structure of (a) $Co_5(OH)_8(chdc)\cdot 4H_2O$ and (b) $Co_5(OH)_8(chdc)$ ($chdc^{2-}$ = *trans*-1,4-cyclohexanedicarboxylate). Green, gray, and red spheres represent Co, C, and O atoms, respectively; H atoms are omitted for clarity. Adapted from ref. 83.

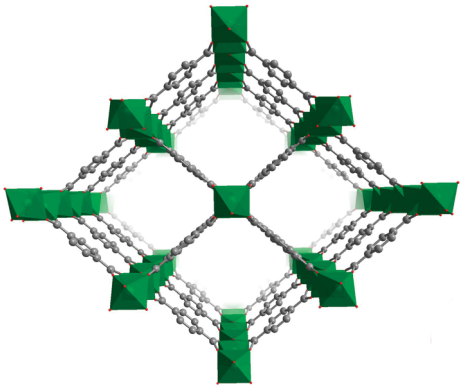

Fig. 8 Polyhedral representation of a portion of the crystal structure of VO(bdc) (MIL-47) showing the 1-D channels (bdc^{2-} = 1,4-benzenedicarboxylate). Green, gray, and red spheres represent Co, C, and O atoms, respectively; H atoms are omitted for clarity.

previous compounds, these layers order ferromagnetically below 60.5 K, giving rise to an overall ferrimagnet. Both hydrated and dehydrated forms exhibit the same ordering temperature. Further investigations performed on single crystals indicate that the magnetic moments lie in the plane of the layer with a large anisotropy, giving rise to very large coercive fields (up to 22 kOe at 2 K). This orientation of the moments is consistent with the high ordering temperature in comparison to the quite large distance between the layers.

Other 2-D inorganic networks are found in the cyanide-based family $[Ni(1,1\text{-dmen})_2]_2[Fe(CN)_6]X\cdot nH_2O$,[84] where 1,1-dmen is 1,1-dimethylethylenediamine, X^- is PF_6^-, BF_4^-, $CF_3SO_3^-$, ClO_4^-, $C_7H_5O_2^-$, I^-, NCS^-, N_3^- or NO_3^-, and n ranges from 2 to 6, depending on X. These structures (I^2O^0) are composed of 2-D square grids, where the ferricyanide nodes are connected by $[Ni(1,1\text{-dmen})_2]^{2+}$ through cyanide linkers. These ferromagnetic grids are separated by the counter-anions and water molecules. The overall magnetic property is governed by the intersheet separation: large intersheet separations (>10 Å) provide ferromagnets (T_c = 9.3–16.2 K), whereas small intersheet separations provide metamagnets (T_N = 11.0–18.3 K) owing to weak intersheet antiferromagnetic interactions that can be overcome by application of a magnetic field. Dehydration of the ferromagnets shortens the intersheet separation, affording therefore metamagnets.

4. Porous magnets based on 1-D inorganic subnetworks (I^1O^n)

The separation of 1-D inorganic chains by organic linkers along the two other dimensions (I^1O^2) is a very efficient way to achieve high porosity through the formation of 1-D channels. Well known examples are $[V^{IV}O(bdc)]$,[85] or MIL-47, and [Cr(OH)(bdc)],[86] or MIL-53(Cr). The structures consist of corner-sharing MO_6 octahedra forming oxo- or hydroxo-bridged chains that are connected by 1,4-benzenedicarboxylate ligands (Fig. 8). The resulting 3-D frameworks offer large 1-D diamond-shaped pores with cross dimensions of 10.0 × 11.5 Å for MIL-47 and 9.4 × 11.3 Å for MIL-53, respectively. Upon evacuation of the guests from the pores, the materials exhibit BET surface areas of 930 and 1100 $m^2\ g^{-1}$, respectively. These microporous solids are able to adsorb large amounts of gases such as CO_2,[87,88] H_2,[89,90] N_2,[85,86] H_2S,[91] CH_4,[87] and small alkanes.[92] Furthermore, these frameworks are highly flexible: the reversible hydration of MIL-53 is followed by a pronounced breathing effect, with the pores closing in the presence of water molecules.[93] Magnetic susceptibility measurements indicate strong antiferromagnetic interactions with large Curie–Weiss constants θ of −186(4) K for MIL-47·$0.75H_2bdc$ and −75 K for MIL-53·H_2O.

Nevertheless, since the large majority of organic linkers used to make porous compounds are unable to mediate a strong magnetic coupling, the appearance of long range order usually occurs only at very low temperatures (see Table 1).

Of course, fascinating magnetic behavior can occur in the absence of long-range magnetic ordering. In particular, for 1-D systems, single-chain magnets can be obtained as a consequence of a large magnetic anisotropy. For such compounds, magnetically isolated chains are highly desirable. The compound $Co_2(H_{0.67}bdt)_3\cdot 20H_2O$ (H_2bdt = 5,5′-(1,4-phenylene)bis(1H-tetrazole)) represents an example of a microporous solid exhibiting single-chain magnet behavior.[95] Its structure is based on inorganic $Co^{II}(\text{–N–N–})_3Co^{II}$ chains separated by the organic ligands, and offers large rectangular channels filled by water molecules. The slow magnetic relaxation, revealed by ac magnetic susceptibility measurements, is confirmed by the presence of a hysterisis loop at 1.8 K with a coercitive field of 450 Oe. The water molecules can be evacuated, affording a microporous solid (SA_{BET} = 729 $m^2\ g^{-1}$) capable of adsorbing gases such as H_2. Similarly, single-chain magnet behavior was also observed in $[Co_3(OH)_2(btca)_2]\cdot 3.7H_2O$ (H_2btca = benzotriazole-5-carboxylic acid).[96] Interestingly, the relaxation barrier for the chains in this compound reversibly disappears upon dehydration. This is due to the appearance of a weak antiferromagnetic coupling between the adjacent ferrimagnetic chains through the aromatic btca ligand, giving rise to a canted antiferromagnet below 4.5 K. The weak interchain coupling can be suppressed by application of a magnetic field, to result in a ferrimagnet-like state.

Besides these 3-D organic/inorganic frameworks, magnetic sponges based on 1-D inorganic networks have also been

reported.[78] An interesting example is the cyanide-bridged heterobimetallic chain $[(Tp)Fe(CN)_3]_2Co$, formed upon the reversible single-crystal-to-single-crystal desolvation of $[(Tp)Fe(CN)_3]_4[Co(CH_3CN)(H_2O)_2]_2 \cdot 10H_2O \cdot 2CH_3CN$ (Tp^- = hydrotris(pyrazolyl)borate).[97,98] The solvated phase is built up from hexanuclear clusters and behaves as a paramagnet. Upon desolvation, new coordination bonds are formed between the ferricyanide moieties and the Co^{II} centers, leading to ferromagnetic double zig-zag chains. A weak antiferromagnetic coupling occurs between the chains below T_N = 4.0 K, which can be overcome with a critical field of 4.5 kOe. The desolvated phase also presents very small empty channels (1.9 × 3.6 Å) capable of adsorbing selectively H_2 and CO_2, but almost no N_2 because of its larger kinetic diameter (3.64–3.80 Å) compared to the effective pore size.

5. Porous magnet without inorganic subnetworks (I^0O^n)

A multitude of highly porous materials have been generated through the connection of metal-based nodes by organic linkers. The interest for these porous coordination solids or metal–organic frameworks (MOFs) comes not only from the capability to reach very high surface areas, but also from their large diversity made possible by a suitable design of the organic linkers. However, the paramagnetic metal-based centers, which can be mono- or polynuclear, are often too isolated to engage in strong magnetic exchange, which generally precludes the occurrence of long range magnetic ordering. This is one of the main reasons why most of the reported MOFs have not been characterized magnetically. Of course, it should be noted that the absence of long range order does not preclude the occurrence of fascinating magnetic properties such as single-molecule magnetism, spin crossover, photomagnetism as well as their related guest-dependent magnetic behavior.[99–105]

Most of the MOFs exhibiting long range magnetic ordering at low temperature are based on small organic linkers (typically three atom bridges).[106–112] Relevant examples are $Co(F\text{-}pymo)_2(H_2O)_{2.5}$ (F-pymo$^-$ = 5-fluoropyrimidin-2-olate)[106] and $Cu(F\text{-}pymo)_2(H_2O)_{1.25}$,[107] which order antiferromagnetically at 29 and 24 K, respectively, with a spin canting for the latter. Both structures are built up from the connection of Co^{II} or Cu^{II} centers through the nitrogen atoms of F-pymo$^-$, forming three-dimensional networks with a sodalite and gismondine topology, respectively (Fig. 9a and b). All of the water molecules can be reversibly evacuated upon heating, affording microporous solids able to adsorb selectively small gas molecules. For the Co compound, further heating induces irreversible polymorphic transformations into nonporous layered phases (Fig. 9c), which exhibit a weak ferromagnetic ordering below 17 K, arising from spin-canting. Due to the small size of the channels, gas adsorption measurements revealed that $Cu(F\text{-}pymo)_2$ is able to adsorb selectively H_2 and CO_2 over N_2, with densities comparable to that of the liquid for H_2 (0.023 *vs.* 0.021 molecules Å^{-3}) and to that of the solid for CO_2 (0.014 *vs.* 0.022 molecules Å^{-3}). The CO_2 adsorption is also responsible for an increment of T_N from 22 to 29 K (Fig. 9d). This selectivity is also observed with $Co(F\text{-}pymo)_2$, which is able to adsorb CO_2, but not N_2, H_2, or CH_4.

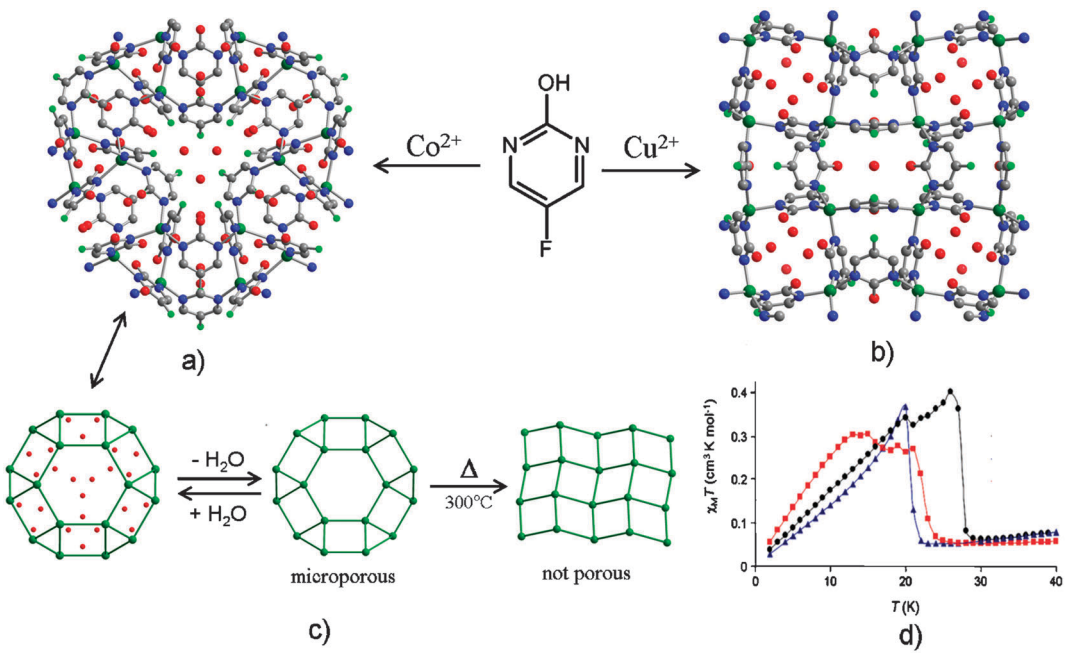

Fig. 9 (a) Portions of the crystal structures of $Co(F\text{-}pymo)_2(H_2O)_{2.5}$ and (b) $Cu(F\text{-}pymo)_2(H_2O)_{1.25}$. Dark green, gray, blue, light green, and red spheres represent Co or Cu, C, N, F, and O atoms, respectively; H atoms are omitted for clarity. (c) Representation of the structural transformations of $Co(F\text{-}pymo)_2(H_2O)_{2.5}$. Dark green and red spheres represent Co and O atoms, respectively, green sticks represent the intermetallic connections through the bridging F-pymo$^-$ ligand. (d) Plots of $\chi_M T$ *vs.* T plot for $Cu(F\text{-}pymo)_2(H_2O)_{1.25}$ (red squares), activated $Cu(F\text{-}pymo)_2$ (blue triangles), and $Cu(F\text{-}pymo)_2$ loaded with CO_2 (black circles) in an applied magnetic field of 100 Oe. Adapted from ref. 106 and 107, copyright American Chemical Society.

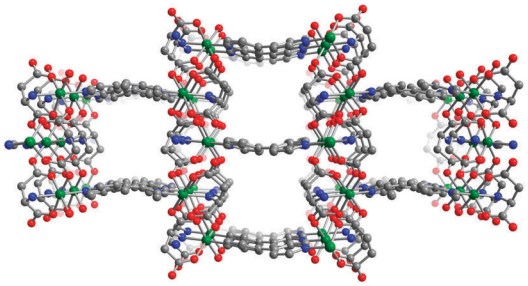

Fig. 10 Portion of the crystal structure of Co_2(L-asp)$_2$(4,4′-bpy)·1.5H_2O showing the parallelepiped channels. Green, gray, blue, and red spheres represent Co, C, N, and O atoms, respectively; H atoms and water molecules are omitted for clarity.

The homochiral metal–organic framework Co_2(L-asp)$_2$-(4,4′-bpy) is another example of porous magnet of the type I^0O^3.[108] This compound is built up from the connection of Co^{II} centers by L-aspartate dianions, forming neutral layers that are pillared by 4,4′-bipyridine linkers (Fig. 10). The resulting 3-D coordination network contains parallelepiped channels originally filled by water molecules. After evacuation, the microporous solid is capable of adsorbing up to 1.48 wt% of H_2 at 1 bar and 77 K. Magnetic measurements performed on the hydrated form of the compound revealed a canted antiferromagnetic order below 14 K, with a small reported hysteresis at 1.9 K (H_c = 72 Oe and M_r = 0.04 μ_B).

Polynuclear clusters have often been used as secondary building units for the formation of porous materials. However, few of the resulting materials present a long-range magnetic order. The compound $KCo_7(OH)_3$(1,3-bdc)$_6(H_2O)_4$·12H_2O (1,3-bdc^{2-} = 1,3-benzenedicarboxylate) possesses a 3-D framework based on heptanuclear oxo-bridged Co^{II} clusters linked *via* 1,3-bdc^{2-} bridging ligands.[113] The compound does not display a long range magnetic order, but behaves as a single-molecule magnet with magnetically isolated Co_7 clusters. Ac susceptibility measurements at different frequencies revealed thermally activated relaxation with a barrier of U_{eff} = 102 K and a preexponential factor of $\tau_0 = 1.36 \times 10^{-10}$ s. A hysterisis loop was also reported at 2 K with H_c = 1600 Oe and M_r = 0.79 μ_B. All of the water molecules can be reversibly removed through a single crystal-to-single crystal transformation, providing a void space of 36% of the total volume, together with a Langmuir surface area of 513 m^2 g^{-1}. The dehydrated phase behaves as a paramagnet.

Recently another cobalt cluster-based porous solid, [$Co_8(\mu_4$-O)Q_{12}]$(NO_3)_2$·16H_2O (HQ = 8-hydroxyquinoline), was reported.[114] This ionic molecular solid, of the type I^0O^0, consists of large sphere-like octanuclear dications with a diameter of *ca.* 2 nm, connected *via* face-to-edge π–π interactions to form a diamondoid supramolecular network. As a consequence of the loose packing of the large cations, a large portion of the crystal (26%) defines a diamondoid channel network. The channel structure is composed of large tetrahedral cavities (diameter = 10 Å) and small apertures (4.3 Å), which are occupied by nitrate counteranions and guest water molecules. Interestingly, the latter can be removed to yield a microporous solid with a Langmuir surface area of 310 m^2 g^{-1}, which is capable of selectively adsorbing CO_2 over CH_4 (40.7 cm^3 g^{-1} against 2.4 cm^3 g^{-1} at 1 bar and 298 K). Despite the long intermolecular Co···Co distances (8.12 Å), a long range magnetic order occurs below 5.2 K, presumably arising *via* exchange coupling through the inter-cluster π–π interactions. For the hydrated form, this spin canted antiferromagnetic ordering appears at a slightly higher temperature of 6.5 K. A small hysterisis loop was also reported at 2 K with H_c = 207 Oe and M_r = 0.036 μ_B.

As previously mentioned, the introduction of polytopic diamagnetic molecules as linkers between the metal-based nodes can considerably enhance the porosity-related features of the material, but is also typically detrimental to the occurrence of a long range magnetic order, these ligands being usually unable to mediate a strong magnetic coupling. The use of paramagnetic organic linkers, acting as magnetic relays, constitute one of the most promising strategy for the design of efficient microporous magnets. This approach will be discussed in the next section.

6. Strategies for the formation of porous magnets

Through the previously discussed examples, we have noticed several methods that can be considered for the formation of microporous magnets. For purely inorganic materials, the introduction of pores can sometimes be achieved by using structure directing agents, or templates. It should be noted that a quite similar method has also been used recently for the formation of a mesoporous inorganic solid that behaves as a magnet at room temperature.[115] Porous cobalt ferrite ($CoFe_2O_4$) was indeed obtained by a simple sol–gel method using an array of polymeric colloidal spheres acting as sacrificial templates (average diameter 0.4 μm). After sintering at 700 °C under O_2, porous $CoFe_2O_4$ formed, offering ordered interconnected spherical pores with an average diameter of 342 nm and 110–130 nm apertures. Magnetic measurements indicate an ordering temperature of *ca.* 300 K, with a very large coercive field of 1.41 T at 10 K. Interestingly, these magnetic features are compared to those of the bulk congener sintered at 1000 °C, and demonstrate a lower H_c and T_c for the bulk sample (0.6 T and 240 K respectively). This simple and efficient method appears however limited by the low available surface area (SA_{BET} = 25.3 cm^2 g^{-1}) inherent to the large size of the pores. Nevertheless, very promising preliminary results towards the magnetic separation of ions have been reported.

The introduction of organic linkers between inorganic layers or chains to form hybrid inorganic/organic materials is also often cited as another strategy for the formation of porous magnet. This approach is a compromise between a purely inorganic material, potentially able to reach high T_c, and highly porous metal–organic frameworks (I^0O^n). Despite some intriguing successes, the magnetic ordering temperatures for most of these compounds are very low.

One of the most promising strategies for inducing long range magnetic ordering in metal–organic frameworks, and possibly enhancing T_c, is without doubt through the introduction of paramagnetic organic linkers. A remarkable example was illustrated with Cu_3(PTMTC)$_2$(pyridine)$_6$(EtOH)$_2$(H_2O)·10EtOH·6H_2O (MOROF-1) by using radical polychlorinated

triphenylmethyl tricarboxylate ($PTMTC^{3-}$) as paramagnetic organic linkers between the metal centers (Fig. 11a).[14]

The structure consists of a 2-D honeycomb network composed of a ring of six metal units and six $PTMTC^{3-}$ radical anions (Fig. 11b). Each Cu^{II} center is coordinated by two monodentate carboxylate groups, two pyridine ligands and one ethanol or water molecule. Due to weak π–π and van der Waals interactions, the packing of these 2-D honeycomb networks is eclipsed along the third dimension, leading to the formation of large 1-D hexagonal channels (Fig. 11c). The latter are filled by water and ethanol molecules and occupy 65% of the total unit cell volume. The most intriguing feature of this structure is the observation of a long range magnetic order below 2 K, in spite of the long distances between the metal-based spin carriers (the distances between Cu^{II} centers are about 15 Å within the layers and 9 Å between them). This may be attributed to the presence of the organic radicals acting as magnetic relays between the metals (the distance between

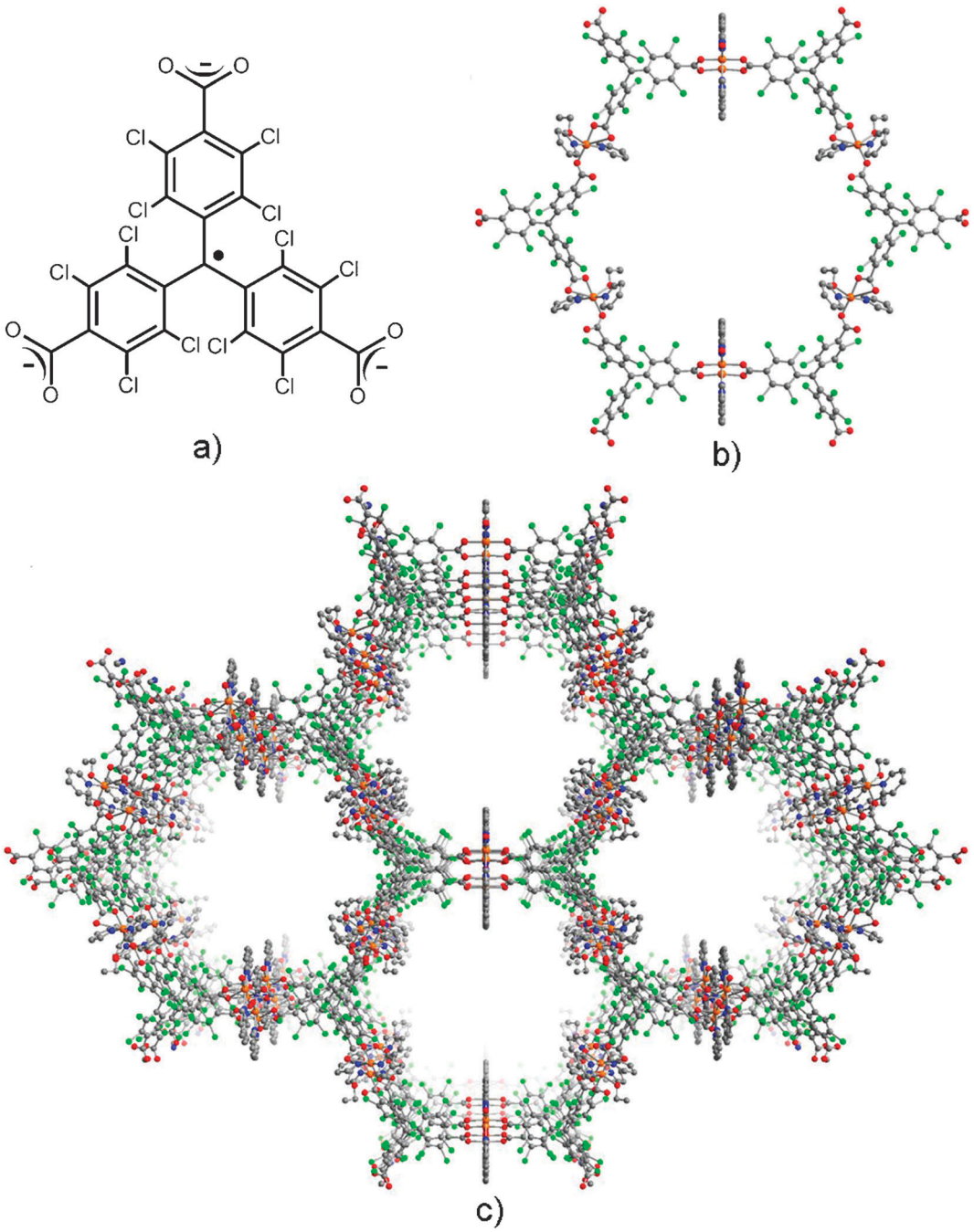

Fig. 11 (a) The polychlorinated triphenylmethyl tricarboxylate radical trianion ($PTMTC^{3-}$). (b) Portion of the crystal structure of the 2-D network resulting from the interconnection of $PTMTC^{3-}$ and Cu^{2+} in $Cu_3(PTMTC)_2(pyridine)_6(EtOH)_2(H_2O)\cdot 10EtOH\cdot 6H_2O$ (MOROF-1). Orange, green, gray, blue, and red spheres represent Cu, Cl, C, N, and O atoms, respectively; H atoms and guest solvent molecules are omitted for clarity. Note that some of the Cu atoms are disordered over two sites. (c) Packing of the 2-D networks giving rise to 1-D nanochannels.

Cu^{II} centers and the central C atom of $PTMTC^{3-}$ is *ca.* 8.3 Å). The magnetic coupling between the Cu and $PTMTC^{3-}$ is antiferromagnetic ($J/k_B = -22$ K), leading therefore to a ferrimagnet. The lattice solvent molecules can be evacuated through a reversible crystalline-to-amorphous transformation involving a shrinking of more than 30% of the total volume. The evacuated sample behaves as a paramagnet.

The room temperature molecule-based magnet $V(TCNE)_x$ (TCNE = tetracyanoethylene) clearly indicates the great potential for using organic radicals as linkers between paramagnetic metal ions.[11–13] Indeed, this solid, of formula $V^{II}(TCNE^{\bullet -})_z(TCNE^{2-})_{1-(z/2)}$ ($1 < z < 2$), behaves as a ferrimagnet with $T_N \approx 400$ K. Due to its amorphous and inhomogeneous nature, the exact structure of this magnet is still not elucidated, even if structural propositions for the limiting forms have been formulated based on spectroscopic and magnetic data.[13] The comparison with similar crystalline compounds, such as $Fe(TCNE)_2 \cdot nCH_2Cl_2$ ($n \approx 0.32$; $T_N \approx 100$ K), provide further clues as to its structural composition. Rietveld refinement performed on synchrotron powder diffraction data show that the structure of the Fe compound is built up from layers of Fe^{II} centers connected *via* μ_4-$TCNE^{\bullet -}$ radical bridges. These layers are connected in the third dimension by diamagnetic μ_4-$[C_4(CN)_8]^{2-}$ units resulting from the dimerization of $TCNE^{\bullet -}$ radicals through the formation of C–C bonds.[116] The structure also features small interlayer channels filled by CH_2Cl_2 solvent molecules. Although not yet been demonstrated, it is possible that certain $TCNE^{\bullet -}$-bridged frameworks could possess the rigidity and architectural stability to provide permanent porosity.

Several other polycyanide organic linkers have been used with more or less success for the formation of molecular magnetic materials.[117] Like TCNE, some of them are also redox active and able to exist as a radical form, providing potentially efficient paramagnetic organic linkers. Recently, a magnetic sponge based upon 2,5-dimethoxy-7,7,8,8-tetracyanoquinodimethane ($TCNQ(MeO)_2$) was reported.[118] The compound, $[Ru_2(O_2CPh\text{-}o\text{-}Cl)_4]_2[TCNQ(MeO)_2] \cdot CH_2Cl_2$, consists of layers wherein paddlewheel-type $Ru_2(O_2CPh\text{-}o\text{-}Cl)_4^{0/+}$ (o-$ClPhCO_2^-$ = o-chlorobenzoate) units are connected *via* μ_4-$[TCNQ(MeO)_2]^{\bullet -}$ radicals. Interstitial CH_2Cl_2 molecules are located in the void spaces between the layers. Magnetic investigations show strong intralayer interactions between the highly anisotropic diruthenium units and the $[TCNQ(MeO)_2]^{\bullet -}$ radicals, as well as a long-range ordering due to antiferromagnetic interlayer interactions below $T_N = 75$ K. A metamagnetic transition to a field-induced canted antiferromagnetic state occurs, giving rise to large coercive fields up to 1.6 T at 1.8 K. Interestingly, the loss of interstitial CH_2Cl_2 through a reversible single crystal-to-single crystal transformation leads to a dramatic change of the magnetic properties, giving rise to a ferromagnetic coupling between the layers with $T_c = 56$ K.

Using paramagnetic organic linkers appears therefore as a very promising strategy for the design of porous materials featuring long range magnetic ordering and potentially high T_c. Nevertheless, stable radicals that can be used as organic linkers are still scarce, and most of them are not well adapted for inducing a significant porosity. The design and synthesis of new rigid and stable radicals with a well defined and specific coordination geometry is therefore highly desirable for the development of this field.

Similar to organic radical linkers, paramagnetic metal-based spacers can also be used, that is metal-based spin carriers with divergent coordination sites. Up to now, this approach is particularly limited by the fact that the design of such building units often involves the presence of blocking ligands that reduce significantly the potential void space.

In order to increase the ordering temperatures in microporous magnets, a suitable choice of metal centers is obviously essential. Indeed, the nature of the metal will strongly influence the strength of the magnetic exchange coupling. Toward this end, theoretical predictions arising from electronic structure calculations can be implemented as effective tools, as exemplified in particular for the Prussian blue analogues.[53–55] From such studies it is clear that using 4d or 5d transition metal centers can present certain advantages, despite the necessarily low spin configurations. First, the more diffuse metal-based spin orbitals can provide a greater overlap with the bridging ligand orbitals, thereby increasing the strength of the magnetic coupling. Furthermore, the greater spin–orbit coupling with these metal ions can result to a higher anisotropy and thus increase the coercivity of the magnets. Finally, their possible higher coordination numbers (7 or 8) can increase the number of exchange pathways, and consequently T_c. For this reason, hepta- and octacyanometallates have been investigated recently for the formation of molecule-based magnets with high ordering temperatures.[119,120] However, only a few of these have this far been demonstrated to be porous.[73,80]

Finally, it is interesting to note that most of permanent magnets with high ordering temperatures are based on magnetism arising from itinerant electrons,[121–123] instead of classical superexchange. The design of porous molecular magnets based on itinerant electrons is very challenging and has yet to be done. This can potentially be achieved in particular through the formation of Class III mixed-valence molecular networks. The formation of such solids requires symmetrical bridging ligands able to mediate an efficient electron transfer, as well as redox-active metal ions that show minimal geometric differences upon changing oxidation state. When the involved metal centers feature more than one unpaired electron, the delocalization of the extra electron stabilizes a parallel alignment of the spin to satisfy the Hund's rules, giving rise to a ferromagnet. This phenomenon is known as double exchange.[124] The design of such molecular solids can rely heavily upon the results from the numerous studies devoted to electron transfer in mixed valence molecular complexes.[125–129] We envision that the adsorption of guest molecules in such solids might break the symmetry, disrupting the electronic delocalization and hence drastically change the magnetic properties and conductivity, thereby giving rise to potential applications as sensors.

7. Conclusions

The introduction of simple organic bridging ligands along with metal ions revolutionized the fields of both microporous

Table 1 Magnetic and guest sorption properties of microporous materials exhibiting both magnetic order and permanent porosity

Compound[a]	Magnetic order[a]	T_c[a]/K	Other relevant magnetic features	SA_{BET}/ $m^2\ g^{-1}$	Guests taken up	Ref.
3-D inorganic subnetworks						
$Ni_{18}(HPO_4)_{14}(OH)_3F_9(H_3O)_4$-$(NH_4)_4(H_2O)_{12}$ (VSB-1)	CAFM	10.5	T_N can be tuned by doping (partial substitution of Ni by Fe, Mn, Zn, Co) to reach T_N = 20 K with Fe	180	N_2, H_2 (10 $cm^3\ g^{-1}$ at 77 K and 600 Torr), H_2O	17, 20, 22, 23, 25–29
$Ni_{20}[(OH)_{12}(H_2O)_6][(HPO_4)_8$-$(PO_4)_4](H_2O)_{12}$ (VSB-5)	AFM	14	Second magnetic transition at *ca.* 6 K, which possibly involves spin canting	500	N_2, H_2 (60 $cm^3\ g^{-1}$ at 77 K and 600 Torr), H_2O	18, 21, 24
$[Fe_4F_3(PO_4)_4](C_6H_{14}N_2)$ (ULM-19)	AFM	9			H_2O	30, 31
$[Fe_2(OH)(H_2O)(PO_4)_2](NH_4)(H_2O)$	AFM	22			H_2O, MeOH	32
$[Ni_8(HPO_3)_9Cl_3](H_3O)_5$	AFM[d]	8.5[d]	Spin-flop transition at 20 kOe		H_2O	33
$Mn_3(HCOO)_6$	FiM	8.1	Guest dependent modulation of T_N from 4.8 to 9.7 K	240	Adsorbs *ca.* 40 different guests, such as DMF, acetic acid, benzene, naphthalene, tetrathiafulvalene, H_2 (0.9 wt% at 1 bar and 78 K), CO_2 (20 wt% at 1 bar and 195 K), but very little uptake of N_2, Ar and CH_4	34,35,38, 40–44
$Fe_3(HCOO)_6$	FiM	16.1	Guest dependent modulation of T_c from 14.8 to 20.7 K Magnetic hysteresis at 1.9 K with H_c = 700 Oe and M_r = 4 μ_B	385	I_2, furans, benzene, acetonitrile, acetone, N_2, H_2 (0.9 wt% at 10 bar and 78 K)	37, 39–41, 44
$Co_3(HCOO)_6$	CAFM	2		360	N_2	36, 37, 40, 44
$Ni_{20}(glu)_{20}(H_2O)_8$ (MIL-77)	FM	4		346	H_2 (85 cm^3 $H_2\ g^{-1}$ at 77 K and 1 bar)	47, 48
Pyr-VF_3	AFM	5			H_2O	130
$CsNi[Cr(CN)_6]$	FM	75	Ferromagnetic interactions with adsorbed O_2	360	N_2, O_2 (4.6 mmol g^{-1} at 77 K and 100 Torr), H_2O	70
$Cr_3[Cr(CN)_6]_2{\cdot}6H_2O$	FiM	219	Magnetic hysteresis at 5 K with H_c = 110 Oe and M_r = 1200 emu G mol^{-1}. Antiferromagnetic interactions with adsorbed O_2	400	N_2, O_2 (10 mmol g^{-1} at 77 K and 100 Torr), H_2O	70
$Fe_4[Fe(CN)_6]_3$	FM[j]	5.6[j]		550	N_2, small alcohols, H_2 (1.6 wt% at 77 K and 980 Torr), H_2O	62–65
$Co_3[Co(CN)_5]_2$	FiM	38	Magnetic hysteresis at 5 K with H_c = 1160 Oe and M_r = 745 emu Oe mol^{-1}	730	N_2, O_2, H_2 (1.4 wt% at 77 K and 980 Torr), H_2O	62, 66
$Mn_3[Fe(CN)_6]_2$	FiM	9.9			N_2, CO_2, MeOH, EtOH, H_2O	67
$Ni_3[Fe(CN)_6]_2$	FM	24.9			N_2, CO_2, MeOH, EtOH, H_2O	67
$Cu_3[Fe(CN)_6]_2$	FM	21.8			N_2, CO_2, MeOH, EtOH, H_2 (1.79 wt% at 75 K), H_2O	67, 131
$Co_3[Fe(CN)_6]_2{\cdot}xH_2O$	FiM	14.4			N_2, MeOH, EtOH, H_2O	67
$K_{0.2}Mn_{1.4}[Cr(CN)_6]$	FiM	99	T_N can be tuned by partial dehydration		H_2O	68
$Co[Cr(CN)_6]_{2/3}(H_2O)_{4.2}$	FiM	22	Reversible transformation from a ferromagnet (T_c = 28 K with 5.1H_2O) to a ferrimagnet during the partial dehydration, with a color change from pink to blue		H_2O	69
$Mn_2(H_2O)_5Mo(CN)_7$	FM	65	With 4 more H_2O, T_c = 51 K Magnetic hysteresis at 5 K with H_c = 0.85 kOe and $M_r \approx 1.8\ \mu_B$		H_2O	132
$[(Co(C_{15}H_{21}N_3O_2))_2Cr(CN)_6]ClO_4$	FM[h]	12[h]	Magnetic hysteresis at 1.8 K with H_c = 165 Oe and M_r = 4.5 μ_B		H_2O	72
$[Mn(HL)]_2Mn[Mo(CN)_7]_2$	FiM	106	Magnetic hysteresis at 2 K with H_c = 90 Oe and $M_r \approx 4\ \mu_B$	15[b]	N_2, CO, CO_2 (0.27 mmol g^{-1}; 610 $cm^3\ g^{-1}$ at 295 K and 1 bar), H_2O	73

Table 1 (*continued*)

Compound[a]	Magnetic order[a]	T_c[a]/K	Other relevant magnetic features	SA_{BET}/ $m^2\ g^{-1}$	Guests taken up	Ref.
$[Mn(NNdmenH)]Cr(CN)_6$	FiM	60.4	Magnetic hysteresis at 2 K with $H_c = 60$ Oe		H_2O, MeOH	74, 75
$[Mn(pnH)]Cr(CN)_6$	FiM	70	Magnetic hysteresis at 2 K with $H_c \approx 60$ Oe and $M_r \approx 0.7\ \mu_B$. With $2H_2O$, $T_N = 36$ K, $H_c = 10$ Oe and $M_r \approx 0.1\ \mu_B$		H_2O	77
$CoCl_2$(1,4-dioxane)	FM	6	Reversible SCSCT from antiferromagnetic chains ($T_N = 3$ K) into a 3-D ferromagnetic diamondoid framework upon dehydration		H_2O	133
2-D inorganic subnetworks						
$Co_4(SO_4)(OH)_6(dabco)_{0.5}$	AFM[c]	21[c]	Ferrimagnetic order in the inorganic layer, very weak antiferromagnetism between the layers, which can be overcome by an applied field to induce a metamagnetic phase		H_2O	82
$Co_4(SO_4)(OH)_6(en)_{0.5}$	AFM[c]	14[c]			H_2O	81, 82
$Co_5(OH)_8(chdc)$	FiM[g]	60.5[g]	Ferrimagnetic order in the inorganic layer, with ferromagnetic interactions between the layers. Large magnetic hysteresis at 2 K with $H_c \approx 22$ kOe		H_2O	83
$[Ni(cyclam)]_3[W(CN)_8]_2$	AFM	5	Field-induced transition to a canted ferromagnetic phase when $H > 9$ kOe		H_2O	80, 134
$[Mn_2(imH)_2][Nb(CN)_8]$	FiM	62	Magnetic hysteresis at 4.3 K with $H_c = 100$ Oe and $M_r = 1.2\ \mu_B$. With $8H_2O$, $T_N = 25$ K		H_2O	80, 135
$[Ni(dmen)_2]_2[Fe(CN)_6](CF_3SO_3)$	MM	10	Spin flipping with an applied field of 400 Oe. Magnetic hysteresis at 5 K with $H_c = 460$ Oe and $M_r = 7200\ cm^3{\cdot}G\ mol^{-1}$		H_2O	84
1-D inorganic subnetworks						
$Co_2(dobdc)(H_2O)_2$	AFM[h]	8[h]	Field-induced transition to a ferromagnet-like ordered state when $H > 2$ T	1080	N_2, CO_2 (30.6 wt% at 296 K and 1 bar), H_2 (1.7 wt% at 77 K and 1 bar), H_2O	136
$Fe_3(PO_4)(HPO_4)_3(C_2O_4)_{1.5}(H_2en)_{1.5}$	AFM[d]	31[d]			H_2O, MeOH	94
$Ni_7(C_4H_4O_4)_4(OH)_6(H_2O)_3$ (MIL-73)	FiM[i]	20[i]		135	N_2, H_2O	137
$Fe(OH)[C_6H_2(CO_2)_2(CO_2H)_2$ (MIL-82)	AFM	5.5	The weak antiferromagnetic coupling between the chains can be overcome with an applied field of 0.5 T (metamagnetism)	30	N_2, H_2O	138
$[Ni_3(OH)_2(cis\text{-chdc})_2(H_2O)_4]$	FM	4.4	Reversible transformation from a ferrimagnet ($T_N = 2.1$ K) to a ferromagnet during the dehydration		H_2O	139
$Co_3(OH)_2(C_4O_4)_2$	FM	8	Reversible transformation from a antiferromagnet ($T_N = 8$ K) to a ferromagnet during the dehydration. The hydrated form undergoes a transition to a CAFM below 6 K		H_2O	140, 141
$Co_3(OH)_2(btca)_2$	CAFM	4.5	Reversible transformation from a ferrimagnetic single chain magnet to a canted antiferromagnet during the dehydration. Field-induced transition to a ferrimagnetic-like state (metamagnetism)	125	N_2, H_2O	96

Table 1 (*continued*)

Compound[a]	Magnetic order[a]	T_c[a]/K	Other relevant magnetic features	SA_{BET}/ $m^2\ g^{-1}$	Guests taken up	Ref.
$[Fe(Tp)(CN)_3]_4Fe(H_2O)_2Fe$	AFM	7	Reversible transformation from antiferromagnetic hexanuclear clusters to antiferromagnetically coupled ferrimagnetic chains during the dehydration		H_2O, MeCN	142, 143
$[Fe(Tp)(CN)_3]_2Co$	AFM	4	Reversible transformation from paramagnetic hexanuclear clusters to antiferromagnetically coupled ferromagnetic chains during the dehydration. Metamagnetic behaviour with a critical field of 4.5 kOe	154	H_2, CO_2, H_2O, MeCN	97, 98
$Co_3(2,4\text{-pydc})_2(OH)_2$	CAFM	6	Magnetic hysteresis at 2 K with H_c = 200 Oe and M_r = 87 emu Oe mol^{-1}		H_2 (0.70 wt% at 77 K and 1 bar)	144
$Ni_3(cmpa)_2(N_3)_4$	AFM	13.2	Field-induced transition to a ferromagnetic-like ordered state when $H > 2.3$T (metamagnetism). Modulation of T_N and the critical field upon partial or total hydration/dehydration		H_2O	145
$Co_3(OH)_2(dbsf)_2$	FiM	7	Magnetic hysteresis at 2 K with H_c = 8300 Oe and M_r = 1.2 μ_B		H_2O, EtOH	146
0-D inorganic subnetworks						
$Co(F\text{-pymo})_2$	AFM[f]	29[f]	A polymorph is obtained by heating at 300 °C, which orders as a spin-canted antiferromagnet below 17 K		H_2O, CO_2 (7 mmol g^{-1} at 28 bar and 273 K), but no significant adsorption of N_2, CH_4, and H_2	106
$Cu(F\text{-pymo})_2$	CAFM	22	Guest dependent modulation of T_c		H_2O, H_2 (0.56 wt% at 90 K and 900 Torr), CO_2 (7.6 wt% at 273 K and 900 Torr), but no significant adsorption of N_2	107
$Co_2(L\text{-asp})_2(4,4'\text{-bpy})$	CAFM[d]	14[d]	Magnetic hysteresis at 1.9 K with H_c = 72 Oe and M_r = 0.04 μ_B	385	N_2, H_2 (1.48 wt% at 1 bar and 77 K)	108
$[Co_5(im)_{10}]_8$	CAFM[k]	10.6[k]	Magnetic hysteresis at 2 K with H_c = 7200 Oe and M_r = 0.07 μ_B		The compound is homochiral 3-Methyl-1-butanol, ethanol, toluene, xylene	109, 110
$Co_2(ma)(ina)$	CAFM[e]	8[e]	Guest dependent modulation of H_c. Magnetic hysteresis at 2 K with H_c = 93 Oe and M_r = 27 emu Oe mol^{-1} [e]		H_2O, MeOH, $HCONH_2$	111
$Mn_2(bpybc)(ox)_2$	AFM	9.8	With $8H_2O$: T_N = 14.7 K, with a field-induced spin-flop transition at 34 kOe		H_2O, H_2 (0.71 wt% at 77 K and 1 bar) and several aromatic donor guests (hydroquinone, catechol, resorcinol, aniline) through charge transfer interactions giving rise to a dramatic modification of the color	112
$CoCu(obbz)(H_2O)$	FiM	25	With $6H_2O$: 0-D nonmagnet; with $3H_2O$: ferrimagnetic chains without long range ordering; with $1H_2O$: 2- or 3-D ferrimagnet. Magnetic hysteresis at 5 K with H_c = 3 kOe		H_2O	78, 147
$CoCu(obze)(H_2O)$	FiM	20	With $6H_2O$: 0-D nonmagnet; with $3H_2O$: ferrimagnetic chains without long range ordering; with $1H_2O$: 2- or 3-D ferrimagnet		H_2O	78, 93

Table 1 (*continued*)

Compound[a]	Magnetic order[a]	T_c[a]/K	Other relevant magnetic features	SA_{BET}/ $m^2\ g^{-1}$	Guests taken up	Ref.
$CoCu(pbaOH)(H_2O)_2$	FM	38	With $5H_2O$: antiferromagnetically coupled ferromagnetic chains without long range ordering; with $3H_2O$: ferromagnetic order between ferromagnetic chains (T_N = 9.5 K); with $2H_2O$: magnetic hysteresis at 2 K with H_c = 5.66 kOe		H_2O	148
PTMTC (POROF-2)	FM	<2	Magnetic hysteresis at 0.08 K with H_c = 93 Oe and M_r = 27 emu Oe mol^{-1}			149
$[Co_8OQ_{12}](NO_3)_2$	CAFM	5.2	With $16H_2O$: T_N = 6.5 K with a magnetic hysteresis at 2 K with H_c = 207 Oe and M_r = 0.036 μ_B	310[l]	H_2O, CO_2 (40.7 $cm^3\ g^{-1}$ at 1 bar and 298 K) with a high selectivity over CH_4	114
$[Ru_2(O_2CPh\text{-}o\text{-}Cl)_4]_2\ TCNQ(MeO)_2$	FM	56	Reversible transformation from an antiferromagnet (T_N = 75 K) to a ferromagnet upon desolvation		CH_2Cl_2	118

[a] FM = ferromagnet; FiM = ferrimagnet; AFM = antiferromagnet; CAFM = spin canted antiferromagnet; MM = metamagnet; T_c = Curie or Néel Temperature; glu^{2-} = glutarate; en = ethylenediamine; L = *N*,*N*-dimethylalaninol; H_2dsbf = 4,4-dicarboxybiphenylsulfone; F-$pymo^-$ = 5-fluoropyrimidin-2-olate; bdc^{2-} = benzenedicarboxylate; btc^{3-} = benzenetricarboxylate; 2,4-$pydc^{2-}$ = pyridine-2,4-dicarboxylate; $chdc^{2-}$ = cyclohexanedicarboxylate; cyclam = 1,4,8,11-tetrazacyclotetradecane; im^- = imidazolate; $dobdc^{2-}$ = 2,5-dihydroxyterephthalate; $cmpa^-$ = 1-carboxymethylpyridinium-4-acrylate; asp^{2-} = aspartate; Tp^- = hydrotris(pyrazolyl)borate; 4,4′-bpy = 4,4′-bipyridine; H_2bpybc^{2+} = 1,1′-bis(4-carboxybenzyl)-4,4′-bipyridinium; HQ = 8-hydroxyquinoline; dabco = 1,4-diazabicyclo[2.2.2]octane; dmen = 1,1-dimethylethylenediamine; $obbz^{4-}$ = *N*,*N*′-bis-(carboxymethyl)oxamido; $obze^{4-}$ = *N*-(2-carboxyphenyl)-*N*′-(carboxymethyl)oxamido; $pbaOH^{4-}$ = 2-hydroxy-1,3-propylenebis(oxamato); H_2btca = benzotriazole-5-carboxylic acid; *o*-$ClPhCO_2^-$ = *o*-chlorobenzoate; TCNQ(OMe) = 2,5-dimethoxy-7,7,8,8-tetracyanoquinodimethane. [b] This small value is due to the absence of strong interaction with N_2. [c] Measurements performed with 0.5 water molecules per formula unit. [d] Measurements performed with 1.5 water molecules per formula unit. [e] Measurements performed with 2 water molecules per formula unit. [f] Measurements performed with 2.5 water molecules per formula unit. [g] Measurements performed with 4 water molecules per formula unit. [h] Measurements performed with 8 water molecules per formula unit. [i] Measurements performed with 7 water molecules per formula unit. [j] Measurements performed with 14 water molecules per formula unit. [k] Measurements performed with two molecules of 3-methyl-1-butanol per formula unit. [l] Langmuir surface area.

materials and magnetism. From the combination of both properties can also result intriguing features such as guest dependent magnetic behavior. A significant number of porous magnets have been reported so far, with variable performances. Among them, Prussian blue analogues deserve particular mention, since they can feature high surface areas together with magnetic ordering temperatures of up to 240 K. In the future, these multifunctional materials could perhaps find applications as sensors or as media for magnetic separations. However, it is first essential to improve their performances. Several strategies have been considered so far and have been discussed in this review. Of particular interest for applications is the formation of microporous materials that behave as permanent magnets at and above room temperature. Recent progress suggests that this goal may now be within reach.

Acknowledgements

This research was funded through the Center for Gas Separations Relevant to Clean Energy Technologies, an Energy Frontier Research Center funded by the U.S. Department of Energy, Office of Science, Office of Basic Energy Sciences under Award No. DE-SC0001015.

References

1 M. Kurmoo, *Chem. Soc. Rev.*, 2009, **38**, 1353.
2 D. Maspoch, D. Ruiz-Molina and J. Veciana, *Chem. Soc. Rev.*, 2007, **36**, 770; D. Maspoch, D. Ruiz-Molina and J. Veciana, *J. Mater. Chem.*, 2004, **14**, 2713.
3 R. J. Kuppler, D. J. Timmons, Q.-R. Fang, J.-R. Li, T. A. Makal, M. D. Young, D. Yuan, D. Zhao, W. Zhuang and H.-C. Zhou, *Coord. Chem. Rev.*, 2009, **253**, 3042.
4 C. N. R. Rao, A. K. Cheetham and A. Thirumurugan, *J. Phys.: Condens. Matter*, 2008, **20**, 083202.
5 M. Eddaoudi, J. Kim, N. Rosi, D. Vodak, J. Wachter, M. O'Keeffe and O. M. Yaghi, *Science*, 2002, **295**, 469.
6 S. Kitagawa, R. Kitaura and S.-I. Noro, *Angew. Chem., Int. Ed.*, 2004, **43**, 2334.
7 G. Férey, *Chem. Soc. Rev.*, 2008, **37**, 191.
8 L. J. Murray, M. Dincă and J. R. Long, *Chem. Soc. Rev.*, 2009, **38**, 1294.
9 J.-R. Li, R. J. Kuppler and H.-C. Zhou, *Chem. Soc. Rev.*, 2009, **38**, 1477.
10 L. Néel, *Ann. Phys. (Paris, Fr.)*, 1948, **3**, 137.
11 J. M. Manriquez, G. T. Yee, R. S. McLean, A. J. Epstein and J. S. Miller, *Science*, 1991, **252**, 1415.
12 G. C. De Fusco, L. Pisani, B. Montanari and N. M. Harrison, *Phys. Rev. B: Condens. Matter*, 2009, **79**, 085201.
13 J. Miller, *Polyhedron*, 2009, **28**, 1596.
14 D. Maspoch, D. Ruiz-Molina, K. Wurst, N. Domingo, M. Cavallini, F. Biscarini, J. Tejada, C. Rovira and J. Veciana, *Nat. Mater.*, 2003, **2**, 190.
15 G. Férey, *Chem. Mater.*, 2001, **13**, 3084.

16 A. K. Cheetham, C. N. R. Rao and R. K. Feller, *Chem. Commun.*, 2006, 4780.
17 N. Guillou, Q. Gao, M. Nogues, R. E. Morris, M. Hervieu, G. Férey and A. K. Cheetham, *C. R. Acad. Sci. Paris Ser. IIc: Chim.*, 1999, **2**, 387.
18 N. Guillou, Q. Gao, P. M. Forster, J.-S. Chang, M. Noguès, S.-E. Park, G. Férey and A. K. Cheetham, *Angew. Chem., Int. Ed.*, 2001, **40**, 2831.
19 S. H. Jhung, J.-S. Chang, S.-E. Park, P. M. Forster, G. Férey and A. K. Cheetham, *Chem. Mater.*, 2004, **16**, 1394.
20 S. H. Jhung, J. W. Yoon, J.-S. Hwang, A. K. Cheetham and J.-S. Chang, *Chem. Mater.*, 2005, **17**, 4455.
21 S.-J. Liu, H.-Y. Cheng, F.-Y. Zhao, J.-Y. Gong and S.-H. Yu, *Chem.–Eur. J.*, 2008, **14**, 4074.
22 X. Wang and Q. Gao, *Mater. Lett.*, 2005, **59**, 446.
23 J.-S. Chang, S.-E. Park, Q. Gao, G. Férey and A. K. Cheetham, *Chem. Commun.*, 2001, 859.
24 Y. Jiang and Q. Gao, *Mater. Lett.*, 2007, **61**, 2212.
25 P. M. Forster, J. Eckert, J.-S. Chang, S.-E. Park, G. Férey and A. K. Cheetham, *J. Am. Chem. Soc.*, 2003, **125**, 1309.
26 T. W. Woo, E.-J. Oh, S. H. Jhung, J.-S. Chang and S. J. Hwang, *J. Nanosci. Nanotechnol.*, 2010, **1**, 240.
27 S. H. Jhung, J.-S. Chang, Y. K. Hwang, J.-M. Grenèche, G. Férey and A. K. Cheetham, *J. Phys. Chem. B*, 2005, **109**, 845.
28 S. H. Jhung, J.-S. Chang, J. W. Yoon, J.-M. Grenèche, G. Férey and A. K. Cheetham, *Chem. Mater.*, 2004, **16**, 5552.
29 L. Xie, Q. Gao, X. Su, P. Wang and J. Shi, *Microporous Mesoporous Mater.*, 2004, **75**, 135.
30 M. Cavellec, J. M. Grenèche and G. Férey, *Microporous Mesoporous Mater.*, 1998, **20**, 45.
31 M. Cavellec, D. Riou, C. Ninlaus, J.-M. Grenèche and G. Férey, *Zeolites*, 1996, **17**, 250.
32 A. Choudhury and S. Natarajan, *Proc.–Indian Acad. Sci., Chem. Sci.*, 1999, **111**, 627.
33 H. Xing, W. Yang, T. Su, Y. Li, J. Xu, T. Nakano, J. Yu and R. Xu, *Angew. Chem., Int. Ed.*, 2010, **49**, 2328.
34 D. N. Dybtsev, H. Chun, S. H. Yoon, D. Kim and K. Kim, *J. Am. Chem. Soc.*, 2004, **126**, 32.
35 Z. Wang, B. Zhang, H. Fujiwara, H. Kobayashi and M. Kurmoo, *Chem. Commun.*, 2004, 416.
36 Z. Wang, B. Zhang, M. Kurmoo, M. A. Green, H. Fujiwara, T. Otsuka and H. Kobayashi, *Inorg. Chem.*, 2005, **44**, 1230.
37 M. Viertelhaus, P. Adler, R. Clérac, C. E. Anson and A. K. Powell, *Eur. J. Inorg. Chem.*, 2005, 692.
38 B. Zhang, Z. Wang, M. Kurmoo, S. Gao, K. Inoue and H. Kobayashi, *Adv. Funct. Mater.*, 2007, **17**, 577.
39 Z. Wang, Y. Zhang, T. Liu, M. Kurmoo and S. Gao, *Adv. Funct. Mater.*, 2007, **17**, 1523.
40 Z. Wang, B. Zhang, Y. Zhang, M. Kurmoo, T. Liu, S. Gao and H. Kobayashi, *Polyhedron*, 2007, **26**, 2207.
41 Z. Wang, K. Hu, S. Gao and H. Kobayashi, *Adv. Mater.*, 2010, **22**, 1526.
42 H. B. Cui, K. Takahashi, Y. Okano, H. Kobayashi, Z. Wang and A. Kobayashi, *Angew. Chem., Int. Ed.*, 2005, **44**, 6508.
43 H. Cui, Z. Wang, K. Takahashi, Y. Okano, H. Kobayashi and A. Kobayashi, *J. Am. Chem. Soc.*, 2006, **128**, 15074.
44 X.-Y. Wang, Z.-M. Wang and S. Gao, *Chem. Commun.*, 2008, 281.
45 Y.-Q. Tian, Y.-M. Zhao, H.-J. Xu and C.-Y. Chi, *Inorg. Chem.*, 2007, **46**, 1612.
46 A. Cornia, A. Caneschi, P. Dapporto, A. C. Fabretti, D. Gatteschi, W. Malavasi, C. Sangregorio and R. Sessoli, *Angew. Chem., Int. Ed.*, 1999, **38**, 1780.
47 N. Guillou, C. Livage, M. Drillon and G. Férey, *Angew. Chem., Int. Ed.*, 2003, **42**, 5314.
48 N. Guillou, C. Livage, N. Audebrand and G. Férey, *11th European Powder Diffraction Conference, Microsymposium 14*.
49 J. B. Goodenough, *Magnetism and the Chemical Bond*, John Wiley and Sons, New York, 1963.
50 L. M. C. Beltran and J. R. Long, *Acc. Chem. Res.*, 2005, **38**, 325.
51 M. Shatruk, C. Avendano and K. R. Dunbar, *Prog. Inorg. Chem.*, 2009, **56**, 155.
52 S. M. Holmes and S. G. Girolami, *J. Am. Chem. Soc.*, 1999, **121**, 5593.
53 M. Verdaguer, A. Bleuzen, V. Marvaud, J. Vaissermann, M. Seuleiman, C. Desplanches, A. Scuiller, C. Train, R. Garde, G. Gelly, C. Lomenech, I. Rosenman, P. Veillet, C. Cartier and F. Villain, *Coord. Chem. Rev.*, 1999, **190–192**, 1023.
54 H. Weihe and H. U. Güdel, *Comments Inorg. Chem.*, 2000, **22**, 75.
55 E. Ruiz, A. Rodriguez-Fortea, S. Alvarez and M. Verdaguer, *Chem.–Eur. J.*, 2005, **11**, 2135.
56 S. S. Kaye and J. R. Long, *J. Am. Chem. Soc.*, 2005, **127**, 6506.
57 S. Natesakhawat, J. T. Culp, C. Matranga and B. Bockrath, *J. Phys. Chem. C*, 2007, **111**, 1055.
58 M. Avila, L. Reguera, J. Rodríguez-Hernández, J. Balmaseda and E. Reguera, *J. Solid State Chem.*, 2008, **181**, 2899.
59 J. Jiménez-Gallagos, J. Rodríguez-Hernández, H. Yee-Madera and E. Reguera, *J. Phys. Chem. C*, 2010, **114**, 5043.
60 C. P. Krap, J. Balmaseda, L. F. del Castillo and E. Reguera, *Energy Fuels*, 2010, **24**, 581.
61 P. K. Thallapally, R. K. Motkuri, C. A. Fernandez, B. P. McGrail and G. S. Behrooz, *Inorg. Chem.*, 2010, **49**, 4909.
62 S. S. Kaye and J. R. Long, *Catal. Today*, 2007, **120**, 311.
63 G. B. Seifer, *Russ. J. Inorg. Chem. (Transl. of Zh. Neorg. Khim.)*, 1959, **4**, 841.
64 B. Mayoh and P. Day, *J. Chem. Soc., Dalton Trans.*, 1976, 1483.
65 F. Herren, P. Fischer, A. Ludi and W. Hälg, *Inorg. Chem.*, 1980, **19**, 956.
66 L. G. Beauvais and J. R. Long, *J. Am. Chem. Soc.*, 2002, **124**, 12096.
67 R. Martinez-Garcia, M. Knobel and E. Reguera, *J. Phys.: Condens. Matter*, 2006, **18**, 11243.
68 Z. Lü, X. Wang, Z. Liu, F. Liao, S. Gao, R. Xiong, H. Ma, D. Zhang and D. Zhu, *Inorg. Chem.*, 2006, **45**, 999.
69 S. Ohkoshi, K. Arai, A. Yusuke and H. Kazuhito, *Nat. Mater.*, 2004, **3**, 857.
70 S. S. Kaye, H. J. Choi and J. R. Long, *J. Am. Chem. Soc.*, 2008, **130**, 16921.
71 V. Gadet, T. Mallah, I. Castro, M. Verdaguer and P. Veillet, *J. Am. Chem. Soc.*, 1992, **114**, 9213.
72 Y.-Z. Zhang and O. Sato, *Inorg. Chem.*, 2010, **49**, 1271.
73 J. Milon, M. C. Daniel, A. Kaiba, P. Guionneau, S. Brandes and J. P. Sutter, *J. Am. Chem. Soc.*, 2007, **129**, 13872.
74 W. Kaneko, M. Ohba and S. Kitagawa, *J. Am. Chem. Soc.*, 2007, **129**, 13706.
75 M. Ohba, K. Yoneda and S. Kitagawa, *CrystEngComm*, 2010, **12**, 159.
76 Y. Yoshida, K. Inoue and M. Kurmoo, *Inorg. Chem.*, 2009, **48**, 267.
77 Y. Yoshida, K. Inoue and M. Kurmoo, *Inorg. Chem.*, 2009, **48**, 10726; Y. Yoshida, K. Inoue and M. Kurmoo, *Chem. Lett.*, 2008, **37**, 586.
78 O. Kahn, J. Larionova and J. V. Yakhmi, *Chem.–Eur. J.*, 1999, **5**, 3443.
79 S. Horike, S. Shimomura and S. Kitagawa, *Nat. Chem.*, 2009, **1**, 695.
80 B. Sieklucka, R. Podgajny, D. Pinkowicz, B. Nowicka, T. Korzeniak, M. Ba1anda, T. Wasiutynski, R. Pe1ka, M. Makarewicz, M. Czapla, M. Rams, B. Gawe1 and W. Lasocha, *CrystEngComm*, 2009, **11**, 2032.
81 A. Rujiwatra, C. J. Kepert and M. J. Rosseinsky, *Chem. Commun.*, 1999, 2307.
82 A. Rujiwatra, C. J. Kepert, J. B. Claridge, M. J. Rosseinsky, H. Kumagai and M. Kurmoo, *J. Am. Chem. Soc.*, 2001, **123**, 10584.
83 M. Kurmoo, H. Kumagai, S. M. Hughes and C. J. Kepert, *Inorg. Chem.*, 2003, **42**, 6709.
84 M. Ohba, H. Ohkawa, N. Fukita and Y. Hashimoto, *J. Am. Chem. Soc.*, 1997, **119**, 1011.
85 K. Barthelet, J. Marrot, D. Riou and G. Férey, *Angew. Chem., Int. Ed.*, 2002, **41**, 281.
86 F. Millange, C. Serre and G. Férey, *Chem. Commun.*, 2002, 822.
87 S. Bourrelly, P. L. Llewellyn, C. Serre, F. Millange, T. Loiseau and G. Férey, *J. Am. Chem. Soc.*, 2005, **127**, 13519.
88 C. Serre, S. Bourrelly, A. Vimont, N. A. Ramsahye, G. Maurin, P. L. Llewellyn, M. Daturi, Y. Filinchuk, O. Leynaud, P. Barnes and G. Férey, *Adv. Mater.*, 2007, **19**, 2246.
89 F. Salles, D. I. Kolokolov, H. Jobic, G. Maurin, P. L. Llewellyn, T. Devic, C. Serre and G. Férey, *J. Phys. Chem. C*, 2009, **113**, 7802.
90 G. Férey, M. Latroche, C. Serre, F. Millange, T. Loiseau and A. Percheron-Guégan, *Chem. Commun.*, 2003, 2976.

91 L. Hamon, C. Serre, T. Devic, T. Loiseau, F. Millange, G. Férey and G. De Weireld, *J. Am. Chem. Soc.*, 2009, **131**, 8775.
92 P. L. Llewellyn, G. Maurin, T. Devic, S. Loera-Serna, N. Rosenbach, C. Serre, S. Bourrelly, P. Horcajada, Y. Filinchuk and G. Férey, *J. Am. Chem. Soc.*, 2008, **130**, 12808.
93 C. Serre, F. Millange, C. Thouvenot, M. Nogues, G. Marsolier, D. Louer and G. Ferey, *J. Am. Chem. Soc.*, 2002, **124**, 13519.
94 A. Choudhury, S. Natarajan and C. N. R. Rao, *Chem. Mater.*, 1999, **11**, 2316.
95 W. Ouellette, A. V. Prosvirin, K. Whitenack, K. R. Dunbar and J. Zubieta, *Angew. Chem., Int. Ed.*, 2009, **48**, 2140.
96 X.-M. Zhang, Z.-M. Hao, W.-X. Zhang and X.-M. Chen, *Angew. Chem., Int. Ed.*, 2007, **46**, 3456.
97 Y.-J. Zhang, T. Liu, S. Kanegawa and O. Sato, *J. Am. Chem. Soc.*, 2010, **132**, 912.
98 J. Kim, S. Han, K. I. Pokhodnya, J. M. Migliori and J. S. Miller, *Inorg. Chem.*, 2005, **44**, 6983.
99 G. J. Halder, C. J. Kepert, B. Moubaraki, K. S. Murray and J. D. Cashion, *Science*, 2002, **298**, 1762.
100 M. Ohba, K. Yoneda, G. Agusti, M. C. Muñoz, A. B. Gaspar, J. A. Real, M. Yamasaki, H. Ando, Y. Nakao, S. Sakaki and S. Kitagawa, *Angew. Chem., Int. Ed.*, 2009, **48**, 4767.
101 P. D. Southon, L. Liu, E. A. Fellows, D. J. Price, G. J. Halder, K. W. Chapman, B. Moubaraki, K. S. Murray, J.-F. Létard and C. J. Kepert, *J. Am. Chem. Soc.*, 2009, **131**, 10998.
102 S. M. Neville, G. J. Halder, K. W. Chapman, M. B. Duriska, P. D. Southon, J. D. Cashion, J.-F. Létard, B. Moubaraki, K. S. Murray and C. J. Kepert, *J. Am. Chem. Soc.*, 2008, **130**, 2869.
103 S. M. Neville, G. J. Halder, K. W. Chapman, M. B. Duriska, B. Moubaraki, K. S. Murray and C. J. Kepert, *J. Am. Chem. Soc.*, 2009, **131**, 12106.
104 E. Coronado, M. C. Giménez-Lopez, C. Giménez-Saiz and F. M. Romero, *CrystEngComm*, 2009, **11**, 2198.
105 M. B. Duriska, S. M. Neville, B. Moubaraki, J. D. Cashion, G. J. Halder, K. W. Chapman, C. Balde, J.-F. Létard, K. S. Murray, C. J. Kepert and S. R. Batten, *Angew. Chem., Int. Ed.*, 2009, **48**, 2549.
106 S. Galli, N. Masciocchi, G. Tagliabue, A. Sironi, J. A. R. Navarro, J. M. Salas, L. Mendez-Liñan, M. Domingo, M. Perez-Mendoza and E. Barea, *Chem.–Eur. J.*, 2008, **14**, 9890.
107 J. A. R. Navarro, E. Barea, A. Rodriguez-Diéguez, J. M. Salas, C. O. Ania, J. B. Parra, N. Masciocchi, S. Galli and A. Sironi, *J. Am. Chem. Soc.*, 2008, **130**, 3978.
108 P. Zhu, W. Gu, F.-Y. Cheng, X. Liu, J. Chen, S.-P. Yan and D.-Z. Liao, *CrystEngComm*, 2008, **10**, 963.
109 Y.-Q. Tian, C.-X. Cai, Y. Ji, X.-Z. You, S.-M. Peng and G.-H. Lee, *Angew. Chem., Int. Ed.*, 2002, **41**, 1384.
110 Y. Q. Tian, C.-X. Cai, X.-M. Ren, C.-Y. Duan, Y. Xu, S. Gao and X.-Z. You, *Chem.–Eur. J.*, 2003, **9**, 5673.
111 M.-H. Zeng, X.-L. Feng, W.-X. Zhang and X.-M. Chen, *Dalton Trans.*, 2006, 5294.
112 Q.-X. Yao, L. Pan, X.-H. Jin, J. Li, Z.-F. Ju and J. Zhang, *Chem.–Eur. J.*, 2009, **15**, 11890.
113 X.-N. Cheng, W.-X. Zhang, Y.-Y. Lin, Y.-Z. Zheng and X.-M. Chen, *Adv. Mater.*, 2007, **19**, 1494.
114 X.-N. Cheng, W. Xue, J.-B. Lin and X.-M. Chen, *Chem. Commun.*, 2010, **46**, 246.
115 E. K. Lee, W. S. Kima, K. W. Lee, H. Limb, J. I. Lee, H. G Lee and N. H. Hur, *Solid State Commun.*, 2009, **149**, 37.
116 J.-H. Her, P. W. Stephens, K. I. Pokhodnya, M. Bonner and J. S. Miller, *Angew. Chem., Int. Ed.*, 2007, **46**, 1521.
117 K. Murray, *Aust. J. Chem.*, 2009, **62**, 1081, and references herein.
118 N. Motokawa, S. Matsunaga, S. Takaishi, H. Miyasaka, M. Yamashita and K. R. Dunbar, *J. Am. Chem. Soc.*, 2010, **132**, 11943.
119 W. Kosaka, K. Imoto, Y. Tsunobuchi and S. Ohkoshi, *Inorg. Chem.*, 2009, **48**, 4604.
120 K. Tomono, Y. Tsunobuchi, K. Nakabayashi and S. Ohkoshi, *Inorg. Chem.*, 2010, **49**, 1298.
121 J. Kübler, *Theory of Itinerant Electron Magnetism*, Oxford Univ. Press, 2000.
122 *Handbook of Advanced Magnetic Materials*, in *Properties and Applications*, ed. Y. Liu, D. J. Sellmyer and D. Shindo, Springer, 2006, vol. 4.
123 M. Shimizu, *Rep. Prog. Phys.*, 1981, **44**, 329.
124 C. Zener, *Phys. Rev.*, 1951, **82**, 403.
125 J. A. McCleverty and M. D. Ward, *Acc. Chem. Res.*, 1998, **31**, 842.
126 W. Kaim, A. Klein and M. Glöckle, *Acc. Chem. Res.*, 2000, **33**, 755.
127 K. D. Demadis, C. M. Hartshorn and T. J. Meyer, *Chem. Rev.*, 2001, **101**, 2655.
128 J.-P. Launay, *Chem. Soc. Rev.*, 2001, **30**, 386.
129 B. Bechlars, D. M. D'Alessandro, D. Jenkins, A. T. Iavarone, S. D. Glover, C. P. Kubiak and J. R. Long, *Nat. Chem.*, 2010, **2**, 362, and references herein.
130 K. Barthelet, J. Marrot, D. Riou and G. Férey, *J. Solid State Chem.*, 2001, **162**, 266.
131 L. Reguera, C. P. Krap, J. Balmaseda and E. Reguera, *J. Phys. Chem. C*, 2008, **112**, 15893.
132 J. Larionova, R. Clérac, J. Sanchiz, O. Kahn, S. Golhen and L. Ouahab, *J. Am. Chem. Soc.*, 1998, **120**, 13088.
133 Z. Duan, Y. Zhang, B. Zhang and D. Zhu, *J. Am. Chem. Soc.*, 2009, **131**, 6934.
134 B. Nowicka, M. Rams, K. Stadnicka and B. Sieklucka, *Inorg. Chem.*, 2007, **46**, 8123.
135 D. Pinkowicz, R. Podgajny, M. Balanda, M. Makarewicz, B. Gawel, W. Lasocha and B. Sieklucka, *Inorg. Chem.*, 2008, **47**, 9745.
136 P. D. C. Dietzel, Y. Morita, R. Blom and H. Fjellvåg, *Angew. Chem., Int. Ed.*, 2005, **44**, 6354.
137 N. Guillou, C. Livage, W. van Beek, M. Noguès and G. Férey, *Angew. Chem., Int. Ed.*, 2003, **42**, 644.
138 M. Sanselme, J.-M. Grenèche, M. Riou-Cavellec and G. Férey, *Solid State Sci.*, 2004, **6**, 853.
139 M. Kurmoo, H. Kumagai, M. Akita-Tanaka, K. Inoue and S. Takagi, *Inorg. Chem.*, 2006, **45**, 1627.
140 M. Kurmoo, H. Kumagai, K. W. Chapman and C. J. Kepert, *Chem. Commun.*, 2005, 3012.
141 S. O. H. Gutschke, M. Molinier, A. K. Powell and P. T. Wood, *Angew. Chem., Int. Ed. Engl.*, 1997, **36**, 991.
142 J. Kim, S. Han, K. I. Pokhodnya, J. M. Migliori and J. S. Miller, *Inorg. Chem.*, 2005, **44**, 6983.
143 Y.-J. Zhang, T. Liu, S. Kanegawa and O. Sato, *J. Am. Chem. Soc.*, 2009, **131**, 7942.
144 Y.-G. Huang, D.-Q. Yuan, L. Pan, F.-L. Jiang, M.-Y. Wu, X.-D. Zhang, W. Wei, Q. Gao, J. Y. Lee, J. Li and M.-C. Hong, *Inorg. Chem.*, 2007, **46**, 9609.
145 W.-W. Sun, C.-Y. Tian, X.-H. Jing, Y.-Q. Wang and E.-Q. Gao, *Chem. Commun.*, 2009, 4741.
146 W. Zhuang, H. Sun, H. Xu, Z. Wang, S. Gao and L. Jin, *Chem. Commun.*, 2010, **46**, 4339.
147 J. Larionova, S. A. Chavan, J. V. Yakhmi, A. G. Frøystein, J. Sletten, C. Sourisseau and O. Kahn, *Inorg. Chem.*, 1997, **36**, 6374.
148 S. Turner, O. Kahn and L. Rabardel, *J. Am. Chem. Soc.*, 1996, **118**, 6428.
149 D. Maspoch, N. Domingo, D. Ruiz-Molina, K. Wurst, G. Vaughan, J. Tejada, C. Rovira and J. Veciana, *Angew. Chem., Int. Ed.*, 2004, **43**, 1828.